Immunity

HIV-1 VRC01 Germline-Targeting Immunogens Select Distinct Epitope-Specific B Cell Receptors

Graphical Abstract

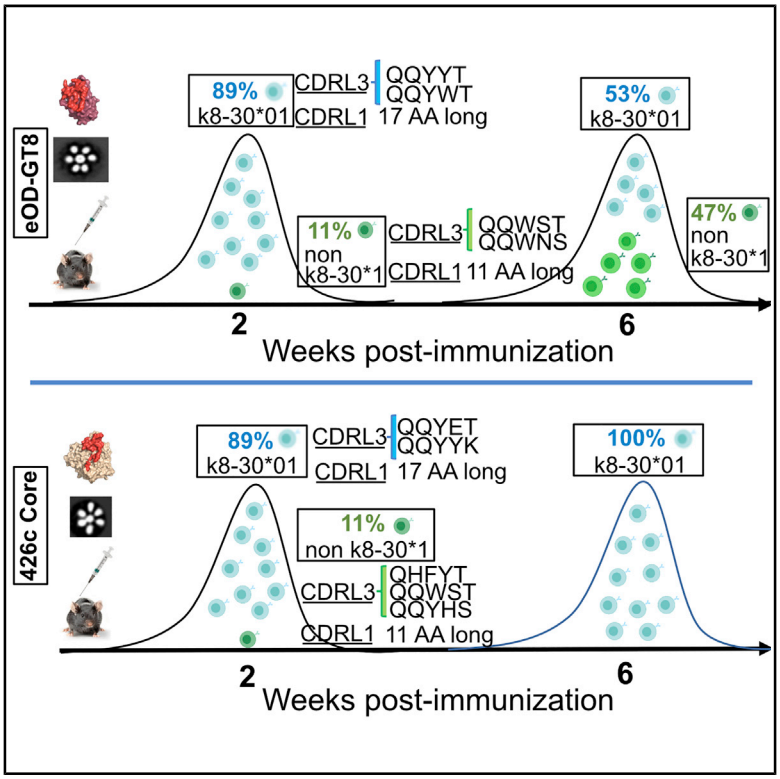

Highlights

- An epitope present on different immunogens selects for different targeted B cells
- Each selected subpopulation comprises B cells with diverse affinities
- The relative affinity dictates the fate of B cells following the initial selection
- Developed 426cOD, a novel VRC01-class germline targeting immunogen

Authors

Yu-Ru Lin, K. Rachael Parks, Connor Weidle, ..., Marie Pancera, Po-Ssu Huang, Leonidas Stamatatos

Correspondence

mpancera@fredhutch.org (M.P.), possu@stanford.edu (P.-S.H.), lstamata@fredhutch.org (L.S.)

In Brief

Activating precursor B cell receptors of HIV-1 broadly neutralizing antibodies requires specifically designed immunogens. Lin, Parks et al. compare three such germline-targeting immunogens against the VRC01-class receptors and find that each immunogen activates VRC01 B cell sub-populations with distinct cross-reactivity properties and that these differences correlate with distinct biophysical and biochemical features of the germline-targeting immunogens.

Lin et al., 2020, Immunity *53*, 840–851
October 13, 2020
https://doi.org/10.1016/j.immuni.2020.09.007

CellPress

CellPress

Immunity

Article

HIV-1 VRC01 Germline-Targeting Immunogens Select Distinct Epitope-Specific B Cell Receptors

Yu-Ru Lin,[1,6] K. Rachael Parks,[1,2,6] Connor Weidle,[1,7] Anika S. Naidu,[3,8] Arineh Khechaduri,[1] Andrew O. Riker,[1] Brittany Takushi,[1] Jung-Ho Chun,[4] Andrew J. Borst,[4] David Veesler,[4] Andrew Stuart,[1] Parul Agrawal,[1] Matthew Gray,[1] Marie Pancera,[1,5,*] Po-Ssu Huang,[3,*] and Leonidas Stamatatos[1,2,9,*]

[1]Fred Hutchinson Cancer Research Center, Vaccines and Infectious Diseases Division, Seattle, WA, USA
[2]University of Washington, Department of Global Health, Seattle, WA, USA
[3]Stanford University, Department of Bioengineering, Stanford, CA, USA
[4]University of Washington, Department of Biochemistry, Seattle, WA, USA
[5]Vaccine Research Center, National Institutes of Allergy and Infectious Diseases, National Institute of Health, Bethesda, MD, USA
[6]These authors contributed equally
[7]Present address: Omeros, Waterfront Research Center, 201 Elliott Ave W, Seattle, WA 98119, USA
[8]Present address: Columbia University Vagelos College of Physicians and Surgeons, New York, NY, USA
[9]Lead Contact
*Correspondence: mpancera@fredhutch.org (M.P.), possu@stanford.edu (P.-S.H.), lstamata@fredhutch.org (L.S.)
https://doi.org/10.1016/j.immuni.2020.09.007

SUMMARY

Activating precursor B cell receptors of HIV-1 broadly neutralizing antibodies requires specifically designed immunogens. Here, we compared the abilities of three such germline-targeting immunogens against the VRC01-class receptors to activate the targeted B cells in transgenic mice expressing the germline VH of the VRC01 antibody but diverse mouse light chains. Immunogen-specific VRC01-like B cells were isolated at different time points after immunization, their VH and VL genes were sequenced, and the corresponding antibodies characterized. VRC01 B cell sub-populations with distinct cross-reactivity properties were activated by each immunogen, and these differences correlated with distinct biophysical and biochemical features of the germline-targeting immunogens. Our study indicates that the design of effective immunogens to activate B cell receptors leading to protective HIV-1 antibodies will require a better understanding of how the biophysical properties of the epitope and its surrounding surface on the germline-targeting immunogen influence its interaction with the available receptor variants *in vivo*.

INTRODUCTION

The development of high-throughput assays to sequence VH and VL paired genes from individual B cells allowed the interrogation of large numbers of antigen-specific B cell receptors (BCRs), prior to and following vaccination or infection (Scheid et al., 2009). Such studies, combined with structural analysis of the antibody-epitope complexes, revealed that broadly neutralizing antibodies (bnAbs) recognize distinct envelope (Env) regions, including the CD4-binding site (CD4-bs), the apex region, the N332 glycan patch and the interface between the gp120 and gp41 subunits (Burton and Hangartner, 2016; Kwong and Mascola, 2012; McCoy and Burton, 2017). Those that bind to the same viral Env epitope can be derived from the same, or very similar, VH and VL pair combinations and have common paratope structures (Chen et al., 2019; Zhou et al., 2013). For instance, the anti-CD4-bs VRC01-class bnAbs are derived from the pairing of VH1-2*02 heavy chains (HCs) and Vλ/Vκs (κ3-20, κ3-15, κ1-33, κ1-5, and λ2-14) light chains (LCs) expressing 5 amino acid-long CDRL3s (Huang et al., 2016; Kwong and Mascola, 2012; Sajadi et al., 2018; Scheid et al., 2011; Umotoy et al., 2019; Zhou et al., 2010; Zhou et al., 2013). They recognize their epitope on Env with similar angles of approach and their paratopes share similar structures, despite being up to 30% divergent in amino acid sequence. Several elements of their VH and VL domains contribute to the strength of their interaction with Env and their breadth of neutralization, but their gene-encoded CDRH2 domains contribute the majority of the antibody buried surface area with Env (Jardine et al., 2016; Zhou et al., 2010), similar to observations made with neutralizing antibodies against other viruses (Chen et al., 2019).

Natural virion-derived Env proteins capable of engaging the unmutated (commonly referred to as "germline", gl) VRC01 BCRs expressed on naive B cells are presently unknown, but specifically designed Env-derived recombinant proteins that bind glVRC01-class antibodies have been engineered (Jardine et al., 2015; McGuire et al., 2016; Medina-Ramírez et al., 2017). These proteins are employed as "gl-targeting" immunogens to activate glVRC01-like BCRs *in vivo* (Dosenovic et al., 2015; Jardine et al., 2015; Parks et al., 2019). It is, however,

expected that subsequent booster immunizations with heterologous, and more native-like, recombinant Env immunogens will be required to guide the maturation of glVRC01 BCRs toward their broadly neutralizing forms (Briney et al., 2016; Dosenovic et al., 2015; Tian et al., 2016).

Here, we examined whether the VRC01 epitope is equally effective in activating glVRC01-expressing B cells *in vivo* when expressed on three different gl-targeting immunogens, eOD-GT8 (Jardine et al., 2015), 426c Core (TM4ΔV1-3) (McGuire et al., 2016), and a newly designed 426c outer domain (426cOD). eOD-GT8 has entered phase I clinical evaluation (NCT03547245), while the 426c Core is scheduled for clinical evaluation in 2021. Despite the difference in binding affinities to glVRC01-class antibodies, all three immunogens were efficient in eliciting VRC01-like antibodies. However, whereas the epitope-specific antibodies elicited by the three immunogens utilized the same VH and VL pairings, they differed at key positions by only a few amino acids and as a result displayed distinct Env cross-reactive properties. Following that initial selection, the relative affinities of the selected BCRs dictated the fate of the corresponding activated B cells. Thus, the initial BCR selection by an immunogenic epitope is critically dependent on its biophysical properties and of its surrounding surface area. Our findings argue that gl-targeting immunogen-design efforts that are solely based on increasing the epitope-exposure on the immunogen or improving the affinity of an antigen are insufficient to accurately predict which target BCRs will be selected during immunization and that the design of more effective immunogens that target the precursor BCRs of protective antibodies will need to take into account the biophysical properties of the epitope and its context.

RESULTS

Design and Characterization of the 426c Env Outer Domain Immunogen

The design of eOD-GT8 is based on the outer domain of the clade B HxB2 Env gp120 subunit (Jardine et al., 2015), while that of 426c Core is based on both the outer and inner domains of the clade C 426c gp120 subunit (McGuire et al., 2016). Here, we engineered a new gl-targeting protein that is derived from the 426c Core but lacks the inner domain (like eOD-GT8), termed 426c outer domain (426cOD). The design of 426cOD was based on that of eOD (which was the universal background of derived variants, such as eOD-GT8) (Jardine et al., 2015; Pejchal et al., 2011) (Figure 1A; Table S1). An initial design (426c base) engineered to bind glVRC01-class monoclonal antibodies (mAbs) was found to bind 1 of 6 gl antibodies (Figure 1B). Random library mutagenesis and yeast-display yielded 426cOD, which binds 4 of 8 glVRC01-class mAbs tested (Figure 1C). We obtained a 3.4 Å X-ray structure of 426cOD bound to mature VRC01 (Figure 2A; Table S2), which confirmed the proper folding of the designed 426cOD (Figure 1D). Comparison with previously published structures of eOD-GT8 and 426c Core (Figure 2B) (Scharf et al., 2016) indicated that VRC01 and glVRC01's epitopes overlapped on each immunogen, and this comparison highlights differences in certain surface exposed residues between 426cOD and eOD-GT8 as follows: $S278R_{gp120}$, $Q361K_{gp120}$, $I370F_{gp120}$, $L455T_{gp120}$, $D457Q_{gp120}$, $D460Y_{gp120}$ (Figures 1A and 2C). These differences translate into different electrostatic surface potentials for the 426c-sequence-based immunogens (negatively charged) compared with eOD-GT8 (positively charged), particularly in the gp120 V5 region that interacts with the CDRH2 and the N terminus of glVRC01 LC (Figure 2C).

To compare the interactions of the 3 antigens (426c Core, eOD-GT8, and 426cOD) with glVRC01, we modeled their interactions by superimposing glVRC01-bound structure with wild-type (WT) 426c Core (PDB ID 6MFT) (Borst et al., 2018) and with eOD-GT6 (PDB ID 4JPK) (Jardine et al., 2013) onto our newly solved structure of 426cOD bound to VRC01. We also modeled glVRC01 binding to eOD-GT8 by superimposing glVRC01 onto VRC01c-HuGL2 bound to eOD-GT8 (PDB ID 5IES) (Jardine et al., 2016). 426cOD buries ~971 $Å^2$ and ~1,007 $Å^2$ upon binding glVRC01 (modeled interactions onto 6MFT and 4JPK, respectively), while eOD-GT8 buries ~1,142 Å2 (modeled interactions onto 5IES) and 426c Core buries ~947 $Å^2$ when binding gl3BNC60 (PDB ID 5FEC) (Scharf et al., 2016). 6–15 estimated H-bonds are formed between modeled glVRC01 and 426cOD (modeled onto 6MFT and 4JPK, respectively). These differences reflect the different conformations adopted by glVRC01 when binding the WT 426 Core (with glycans present) versus the 426c Core (Borst et al., 2018). 21 estimated H-bonds are formed between glVRC01 modeled with eOD-GT8, while 20 estimated H-bonds are formed between 426c Core and gl3BNC60 (PDB ID 5FEC) (Scharf et al., 2016) (Table S3).

The analysis also revealed differences in amino acid exposures between 426c Core and 426cOD when they interact with glVRC01: Val430 in the β20-21 region of gp120, present only in 426c Core, showed some interactions with glVRC01, while Asp48 and Glu49, only present in 426cOD, showed some interactions with VRC01.

The glVRC01 HC buries a larger surface area with 426cOD than eOD-GT8 (Table S4), while the LC buries a larger surface area with eOD-GT8: this is likely because of the LC interactions with bulkier residues present in eOD-GT8 compared with 426cOD: $Arg278_{gp120}$ and $Tyr460_{gp120}$ in eOD-GT8 in place of $Ser278_{gp120}$ and $Asp460_{gp120}$ in 426cOD. The affinity of glVRC01 mAb for 426cOD is in the same range as for 426c Core (289 nM and 217 nM, respectively), while it is <0.1 nM for eOD-GT8 (Figure 1E–1G).

We examined whether differences in affinity influence the efficiency by which the two immunogens select for naive B cells that express VRC01 BCRs *in vivo*, and whether and how the presence of the gp120 inner domain of the 426c Core antigen influences this selection at the molecular BCR level.

Epitope Affinity and the Inner Domain Influences the Efficiency by which Epitope-Specific Naive B Cells Can be Isolated

As orthologs of the human VH1-2*02 gene are not expressed in animal species such as mice, rats, rabbits, and non-human primates (West et al., 2012), the abilities of the 3 antigens to engage glVRC01 BCRs *in vivo* were compared in a well-defined, transgenic mouse model that is heterozygous for the human-inferred gl HC of the VRC01 mAb ($VRC01^{glHC}$) (Jardine et al., 2015). Approximately 80% of B cells express the human transgene

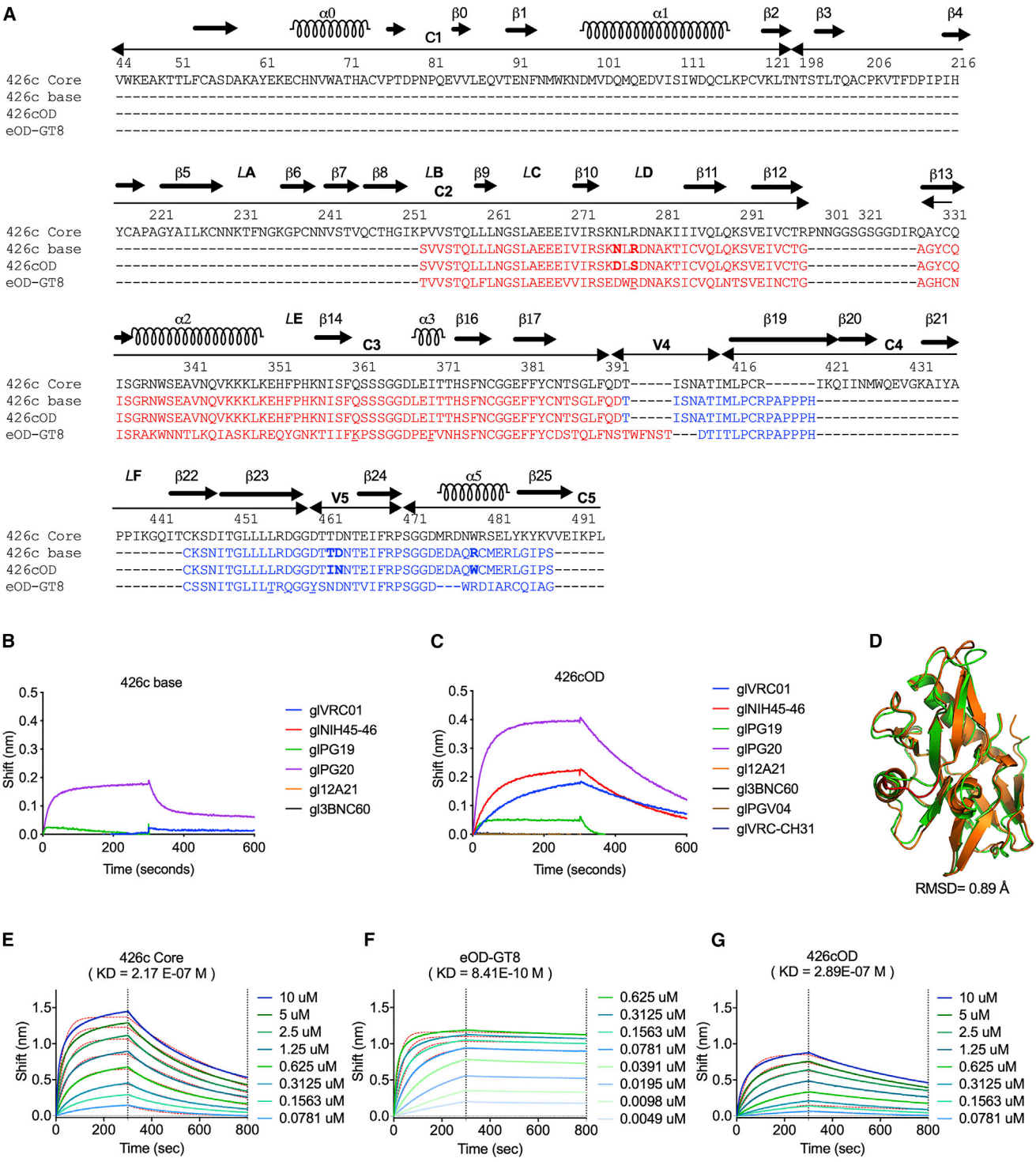

Figure 1. Characterization of 426cOD, Related to Figure S3 and Table S1

(A) Amino acid alignment of 426c Core, 426c base, 426cOD, and eOD-GT8. HxB2 numbering is used. The sequences of 426c base, 426cOD, and eOD-GT8 are reverted to align with that of the 426c Core, as their actual sequences from their N to C termini start with sequences highlighted in blue. Residues that differ between 426c base and 426cOD are shown in bold letters. The residues in eOD-GT8 that differ from those on 426c Core and 426cOD are underlined.

(B and C) BLI was used to evaluate glVRC01-class antibodies binding to 426c base (b) and 426cOD (c). (d) 426c base design model (orange) superimposed onto the 426cOD crystal structure (green). The structural difference between the two is highlighted in red. All atom RMSD is 0.89 Å. (e-g). BLI was used to determine the affinity of germline VRC01 to the three germline-targeting immunogens. The binding curves use to calculate this value are shown. BLI data are representative of at least 2 independent experiments

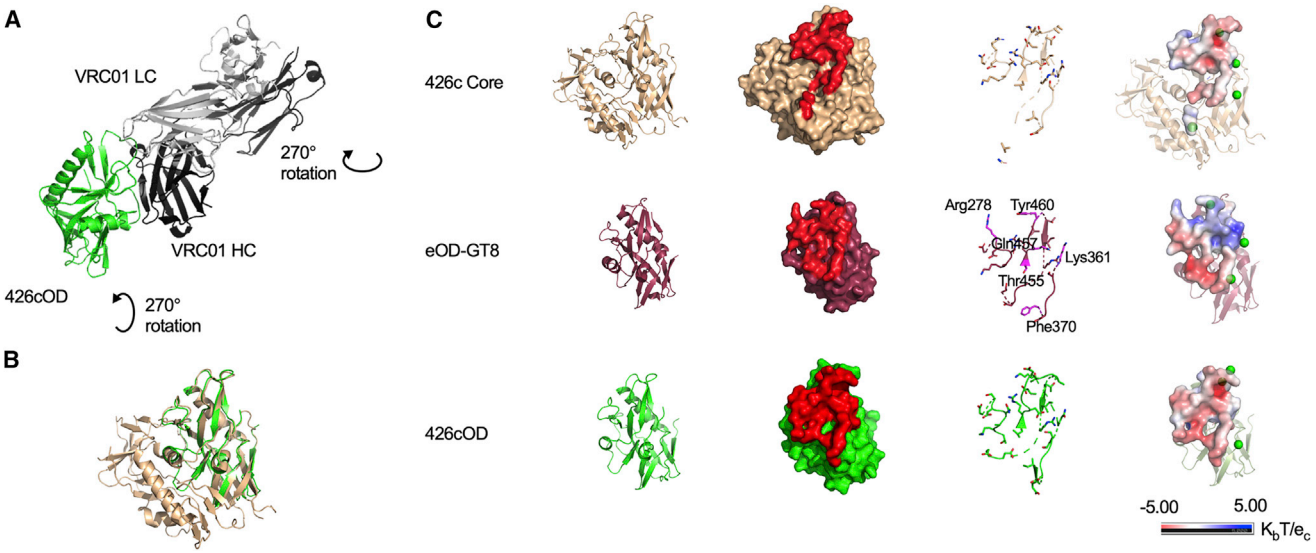

Figure 2. Structures of Three VRC01 Germline-Targeting Immunogens, Related to Tables S2, S3, and S4

(A) Crystal structure of 426cOD (green) bound to human mature VRC01 Fab (light chain in gray, heavy chain in black) shown in cartoon representation.

(B) Overlay of 426c Core (tan, PDB ID 5FA2) and 426c OD (green).

(C) Structural comparison of the three germline-targeting immunogens. From left to right: cartoon representation. Surface representation of immunogens with glVRC01 epitope highlighted in red. glVRC01 epitopes shown in stick representation: eOD-GT8 residues that differ from those on 426c Core and 426cOD are highlighted in magenta. Electrostatic potential of glVRC01 epitopes. The location of potential NLGS around the VRC01 epitope on the three antigens are indicated by green dots (electrostatic potentials do not consider the glycans as exact glycosylation at these positions is unknown).

and all express mouse LCs (mLCs); only 0.01% of which contain 5 amino acid-long CDRL3s. As a result, approximately 0.08% of naive B cells are expected to express VRC01-like BCRs, compared with 0.02% −0.012% of naive human B cells (Abbott et al., 2018; Jardine et al., 2015).

Individual eOD-GT8+/eOD-GT8 CD4-bs KO−, 426c Core+/426c Core CD4-bs KO−, or 426cOD+/426cOD CD4-bs KO− B cells were isolated from the spleens of naive mice. VH and VL genes were then amplified and sequenced. Approximately 62%, 89%, and 61% of HCs isolated with 426c Core, eOD-GT8 and 426cOD, respectively, were VRC01^{glH} (Figure 3A). The vast majority of VRC01^{glHC}-paired mLCs that were selected by either antigen expressed 9 amino acid-long CDRL3s, but mLCs with 6–8 or 10 amino acid-long CDRL3s were also present (Figure 3b). Only the two ''outer domain'' antigens selected for mLCs expressing 5 amino acid-long CDRL3s. We also sorted naive B cells with the C4b-based form of 426c Core from three animals. Out of 282 VL genes that were sequenced, only three LCs with 5 amino acid CDRL3s were identified (one from one animal [0.9%], two from another [1.9%], and none from the third animal [0%] [data not shown]). The isolation of B cells expressing glVRC01-like BCRs by the two ''outer domain-based'' antigens (eOD-GT8 and 426cOD), but not by 426c Core, despite the fact that 426cOD and 426c Core have similar affinities for glVRC01, suggests that the presence of the inner domain limits the accessibility of the VRC01 epitope by BCRs expressed on naive B cells, but not by soluble antibodies. We next examined whether the differences observed in binding to naive VRC01 B cells by the three immunogens had any effect on the ability of the immunogens to expand naive B cells *in vivo*.

Epitope Affinity Does Not Influence the Efficiency by which Epitope-Specific B Cells Expand during Immunization

C4b-based nanoparticle forms (heptameric) of the three antigens were used as immunogens (Hofmeyer et al., 2013). Negative-stain electron microscopy analysis confirmed that all three preparations had similar oligomeric features (Figures S1A–S1C). Two weeks post-immunization, CD4-bs-specific class-switched B cells were single-cell-sorted from spleens and their VH and VL genes sequenced. Approximately 92%, 83%, and 67% of the VHs sequenced from the 426c Core-, eOD-GT8-, and 426cOD-immunized animals, respectively, were VRC01^{glHC} (Figure 3C). Approximately 24%, 34%, and 20% of mLCs from the 426c Core-, eOD-GT8-, and 426cOD-immunized animals, respectively, expressed 5 amino acid-long CDRL3s (Figure 3D). The majority of the mLCs with 5 amino acid-long CDRL3s were derived from κ8-30*1, but κ4-72*01-, κV6-15*01-, κ12-46*01-, κ4−61*01-, and κV4-86*01-derived mLCs were also identified (Figure 3E). Thus, the three immunogens are effective in activating B cells expressing VRC01-like BCRs, despite differences in affinities, as others have reported in the case of model antigens (Kouskoff et al., 1998; Shih et al., 2002). Dosenovic et al., also reported that while tetrameric baits of eOD-GT8 do not identify glVRC01-class B cells in the gl3BNC60 mouse, immunization with the multimeric form of eOD-GT8 results in the activation of such cells (Dosenovic et al., 2015).

Different Env Cross-Reactivity Properties of Plasma Antibodies

Robust autologous plasma antibody responses were elicited by all three immunogens in all animals (Figures 3F–H and S1D–S1F).

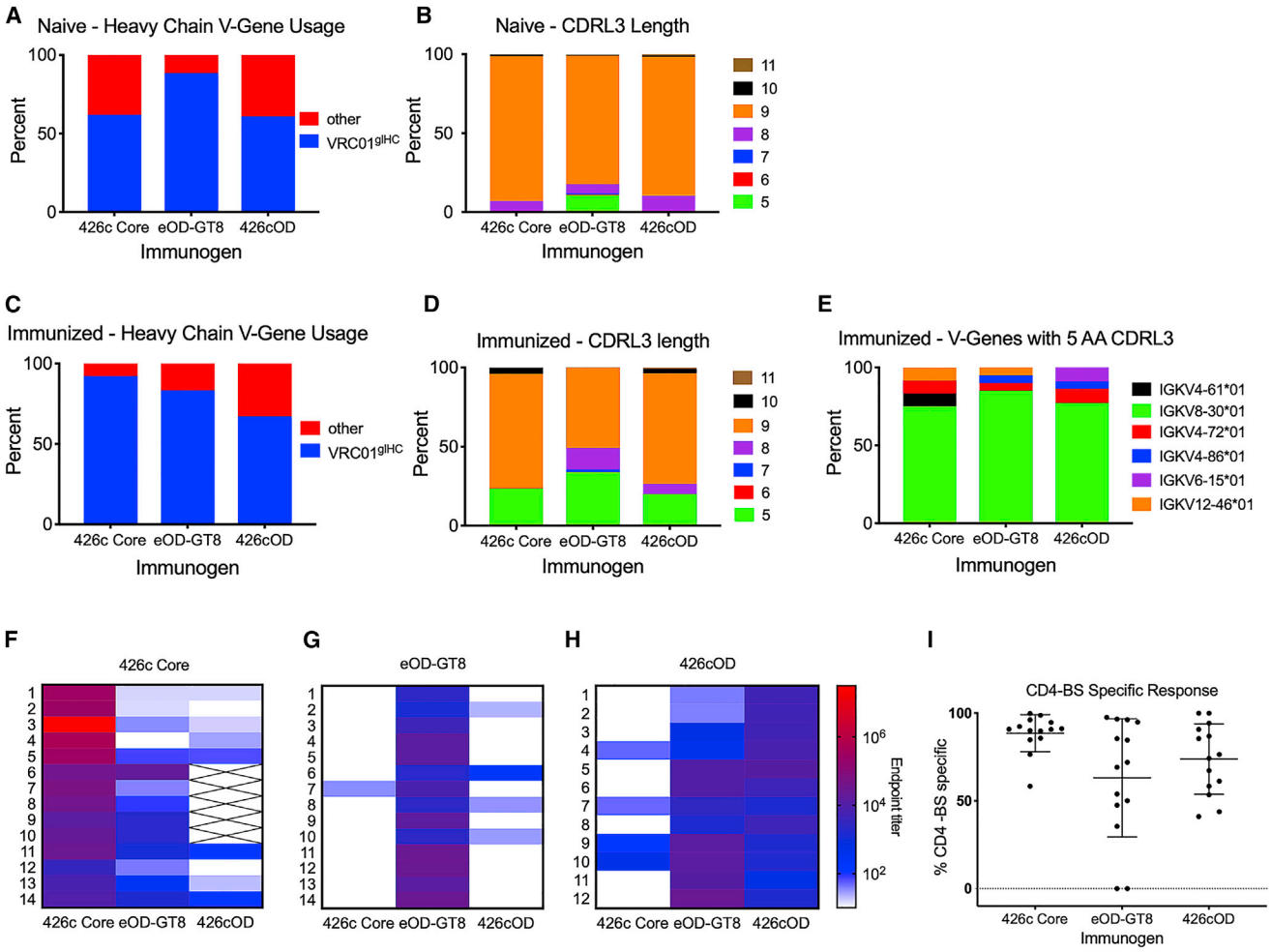

Figure 3. Vaccine Elicited Antibody and B Cell Responses, Related to Figure S2 and Tables S5 and S6

Antigen-specific B cells were sorted and sequenced from naive and immunized animals.

(A and B) VH gene usage (VH sequences: 426c Core n = 21, eOD-GT8 n = 191, 426cOD n = 23) (A) and CDRL3 length (number of sequences: 426c Core n = 98, eOD-GT8 n = 225, 426cOD n = 125) (B) of naive B cells sorted with 426c Core, eOD-GT8 or 426cOD.

(C and D) VH gene usage (number of sequences: 426c Core n = 89, eOD-GT8 n = 48, 426cOD n = 67) (C) and CDRL3 length (number of sequences: 426c Core n = 51, eOD-GT8 n = 59, 426cOD n = 110) (D) of antigen-specific B cells isolated 2 weeks post-immunization.

(E) VL gene usage of 5 AA-long CDRL3 B cells isolated from immunized animals (number of sequences: 426c Core n = 12, eOD-GT8 n = 20, 426cOD n = 22) 2 weeks post-immunization. Percentages indicate the frequency of VH or VL genes with the indicated characteristics out of the total number of VH and VL genes sequenced.

(F–H) ELISAs were performed with plasma from immunized mice. Plasma antibody endpoint titers 2 weeks post immunization with 426c Core (F), eOD-GT8 (G), or 426cOD (H) against 426c Core, eOD-GT8, and 426cOD. Data are shown as a heatmap, with the strongest response (greater endpoint titer) in red. No color indicates undetectable reactivity. X indicates not tested. 12–14 mice immunized with each immunogen were tested. The animal number is indicated to the left of the heatmap.

(I) Percent of plasma antibodies targeting the autologous CD4-BS, elicited by the indicated VRC01 germline-targeting immunogens. Each dot represents an animal. Lines represent mean and standard deviation.

A large proportion of plasma antibody responses targeted the autologous CD4-bs in all three cases (Figure 3I), although 426c Core was more consistent in eliciting such antibodies than the two outer domain immunogens. 13 of 14 animals immunized with 426c Core elicited anti-eOD-GT8 plasma antibody responses (Figure 3F), which recognized the VRC01 epitope on eOD-GT8 (Figure S1D), while only 1 of 14 animals immunized with eOD-GT8 elicited (very weak) anti-426c Core plasma antibody responses (Figure 3G). All animals immunized with 426cOD elicited plasma antibodies against the VRC01 epitope expressed on eOD-GT8, and 4 of 12 animals elicited anti-426c Core plasma antibodies (Figures 3H and S1E). In contrast, only 4 of 14 animals immunized with eOD-GT8 generated anti-426cOD plasma antibodies and with only partial specificity to the CD4-bs of 426cOD (Figures 3G and S1E).

The absence of anti-426c Core antibodies in the plasmas of the eOD-GT8-immunized animals was unexpected, as VRC01-like B cells utilizing the same VH and VL pairings (VRC01^{glHC} and κ8-30*1 mLCs) were isolated in both the 426c Core and eOD-GT8-immunized animals. Antibodies derived from this

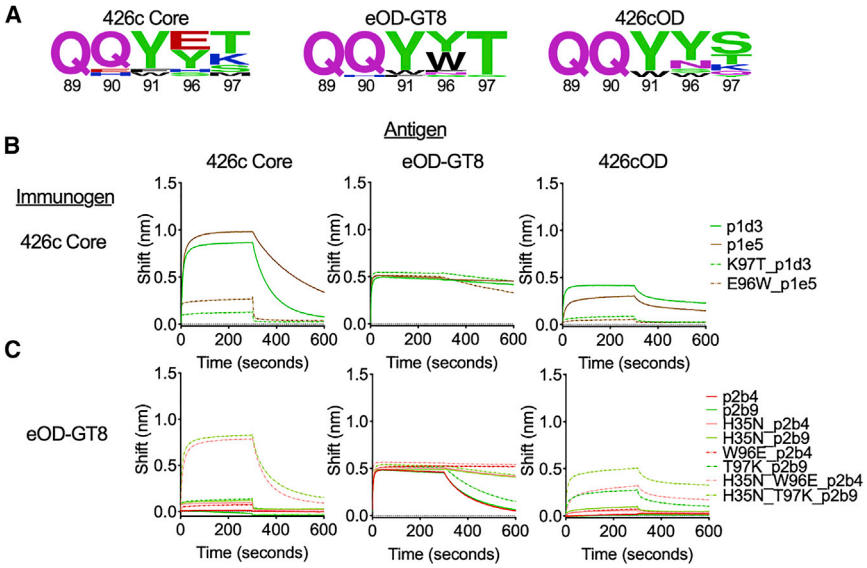

Figure 4. VRC01 Germline-Targeting Immunogens Select for Different Amino Acids within VRC01 BCRs, Related to Table S5

(A) Logo plots represent 5 AA CDRL3 sequences from antigen-specific B cells isolated 2 weeks post-immunization with the indicated VRC01 germline-targeting immunogens. The numbering of the CDRL3 region is based on the Kabat numbering system. Size of amino acid reflects frequency of use.

(B and C) BLI was used to evaluate the binding abilities of mAbs, and of their indicated mutated forms, isolated from 426c Core (B) and eOD-GT8 (C), to the indicated antigens. BLI data are representative of at least 2 independent experiments.

HC-LC pairing from the eOD-GT8- and 426c Core-immunized animals also displayed different cross-reactive properties. Those derived from the eOD-GT8-immunized animals did not bind 426c Core (but bound eOD-GT8 in a VRC01-epitope-dependent manner) (Figure S1E), while those derived from the 426c Core-immunized animals recognized both 426c Core and eOD-GT8 (Figure S1H). In sum, the cross-reactivities of VRC01-like antibodies elicited by 426c Core and by eOD-GT8 differ.

eOD-GT8 and 426c Core Select for Different Variants of VRC01 BCRs

A key difference between the eOD-GT8- and 426c Core-selected κ8-30*01 mLCs with 5 amino acid-long CDRL3s is the selection of different amino acids at the C terminus of the CDRL3 (at the junction of the V and J genes) (Figure 4A). The eOD-GT8-selected CDRL3s with aromatic residues at position 96_{LC} followed by a threonine at position 97_{LC} ($W^{96}T^{97}$or $Y^{96}T^{97}$). As a result, 30% of the 5 amino acid-long CDRL3s had the QQY**WT** motif and 60% had the QQY**YT** motif (Table S5A). This preferential selection was reported by Jardine et al. (Jardine et al., 2015). In contrast, the 426c Core-selected κ8-30*01 mLCs with 5 amino acid-long CDRL3s primarily expressed either a negatively charged amino acid at position 96_{LC} (E^{96}) or a positively charged amino acid at position 97_{LC} (K^{97}). As a result, 50% of the 5 amino acid-long CDRL3s had the QQY**ET** motif and 50% had the QQY**YK** motif (Table S5B). In addition to these differences in the mLCs, most $VRC01^{gIHC}$ sequences from the 426c Core-immunized animals contained a H35N mutation in the CDRH1 (as it exists in mature VRC01), which was not present in the $VRC01^{gIHC}$ sequences from the eOD-GT8-immunized animals. 426cOD displayed a B cell selection phenotype with some similarities to those of eOD-GT8 and 426c Core, as it selected for κ8-30*01 mLCs with 5 amino acid-long CDRL3s with ($W^{96}T^{97}$) (QQY**WT**; 20% of sequences), like eOD-GT8, but also with K^{97} (QQY**YK**; 20% of sequences), like 426c Core (Table S5C). The QQY**YS** sequence was the most prevalent (60% of the sequences). We propose that the positive electrostatic surface around the VRC01 epitope on eOD-GT8 disfavors the selection of CDRL3s with a positively charged amino acid at position 97_{LC} (K^{97}) and that the presence of Y30 on eOD-GT8 (D460 on 426c Core) selects for CDRL3s with aromatic residues at position 96_{LC} to gain enthalpically favorable aromatic ring interaction (Sangesland et al., 2019). We note that the known human VRC01-class bnAbs do not express such bulky amino acids in their CDRL3s (Umotoy et al., 2019; Zhou et al., 2013).

To examine whether the disparate cross-reactivities of the VRC01-like antibodies elicited by the germline-targeting immunogens are due to the selection of different amino acids in their CDRL3 and CDRH1 domains, we performed targeted mutagenesis on the $VRC01^{gIHC}$ and κ8-30*01 genes of two antibodies, p2b4 and p2b9, derived from eOD-GT8-immunized animals and examined how the mutations affected the antibody-binding properties. To this end, we introduced $H35N_{HC}$ or $W96E_{LC}$ on p2b4 and $T97K_{LC}$ on p2b9. While neither p2b4 and p2b9 bound to 426c Core, the individual CDRH1 or CDRL3 substitutions resulted in weak but detectable binding (Figure 4C). Of note, both types of mutations decreased the binding off-rates to eOD-GT8, and p2b4 with the $W96E_{LC}$ mutation displayed negligible off-rate to eOD-GT8. When the CDRH1 and CDRL3 substitutions were simultaneously introduced, the binding of both antibodies to 426c Core became similar to that of VRC01-like antibodies isolated from 426 Core-immunized animals (Figure 4B). Conversely, when the reversed mutations $K97T_{LC}$ or $E96W_{LC}$ were introduced to two $VRC01^{gIHC}$ and κ8-30*01 antibodies (p1d3 and p1e5) isolated from the 426c Core-immunized animals, their binding to 426c Core was drastically diminished, while their binding to eOD-GT8 was unaffected (Figure 4B).

We recently reported that VRC01-like antibodies elicited by 426c Core in this transgenic mouse model can bind to certain heterologous WT gp120 core proteins, even in the presence of N276-associated glycans, which normally prevent the binding of germline VRC01-class mAbs to Env (Parks et al., 2019). These heterologous cores are derived from different clades (93TH057 is clade A/E, Q168a is clade A, and HxB2, 45_01 and QH0692 are clade B), they express a functional N276 glycan site and are not recognized by gIVRC01 (Parks et al., 2019). In agreement, two of eight 426c Core-elicited VRC01-like Abs (p1a6 and p1a7)

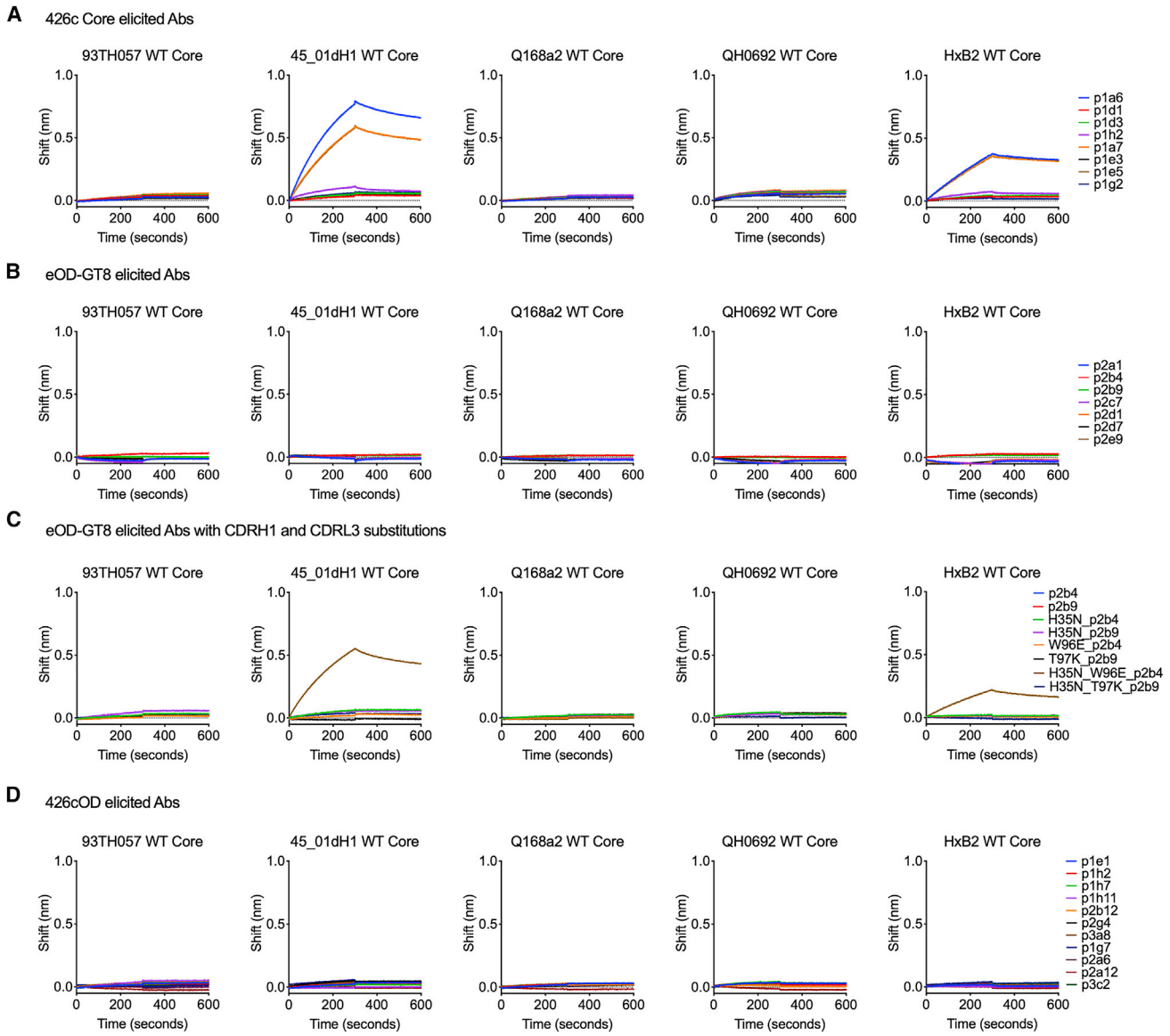

Figure 5. Vaccine Elicited mAbs Binding to Multimeric (C4b-BP) Heterologous Core Env, Related to Figure S1 and Table S5

BLI was used to evaluate binding of mAbs elicited by 426c Core (A), eOD-GT8 (B), and 426cOD (D) to the indicated heterologous wild-type (WT) Core proteins. BLI binding curves are shown. (C) BLI was used to evaluated binding of mAbs elicited by eOD-GT8 with CDRL3 and CDRH1 substitutions to multimeric heterologous Core Env. BLI binding curves (representative of at least two independent experiments) are shown.

recognized two (45_01dH1 WT Core and HxB2 WT Core) of the five heterologous WT core proteins tested (Figure 5A). In contrast, the eOD-GT8-elicited VRC01-like antibodies did not display such cross-reactive reactivities (Figure 5B). We tested the p2b4 and p2b9 mutants for binding to the heterologous WT core proteins and observed that the double substitution on the background of p2b4 (H35N, W96E) conferred cross-reactivity to the two heterologous core proteins recognized by the 426c Core-elicited VRC01-like antibodies (Figure 5C).

Thus, even though eOD-GT8 and 426c Core effectively stimulate naive B cells expressing BCRs composed of VRC01^{glHC} paired with κ8-30*01 mLCs with 5 amino acid-long CDRL3s, they select for different amino acids at positions 96_{LC} and 97_{LC} (Kabat numbering) in the CDRL3 (junction of V and J genes). Additionally, the VRC01^{glHC} from the 426c Core-immunized animals almost universally acquired the H35N mutation. Those few amino acid differences are responsible for differences in the cross-Env recognition potentials of the VRC01-like antibodies elicited by eOD-GT8 and by 426c Core. Our results suggest therefore that VRC01-like antibodies expressing bulky amino acids at position 96_{LC} will not bind effectively the VRC01 epitope on heterologous proteins in the presence of the inner gp120 domain. In agreement with this, VRC01-like antibodies elicited by 426cOD, expressing tyrosine at position 96_{LC}, have no binding to any heterologous WT gp120 core Env proteins (Figure 5D). As the first wave of VRC01-like antibodies elicited by these

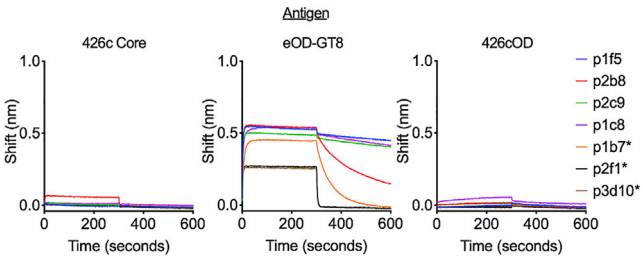

Figure 6. Binding Properties of Monoclonal Antibodies Isolated 6 Weeks Post-immunization with eOD-GT8, Related to Table S5

Monoclonal antibodies isolated 6-weeks post-immunization with eOD-GT8 were evaluated for binding to 426c Core, eOD-GT8, or 426cOD using BLI. mAbs utilizing κ4-61*01 are noted with an asterisk. Data are representative of at least 2 independent experiments.

germline-targeting immunogens are minimally mutated, the antibodies did not display neutralizing activities, in agreement with previous reports (Briney et al., 2016; Parks et al., 2019).

Temporal Evolution of Epitope-Specific VRC01-like B Cell Variants

The germinal center reaction is a dynamic process during which B cell clones compete for antigen and T cell help (Shih et al., 2002; Tas et al., 2016; Victora and Nussenzweig, 2012). To examine whether and how the VRC01-like B cell responses elicited by the three immunogens evolve over time, animals were immunized with the three immunogens, CD4-bs+/KO− B cells were isolated 6 weeks later, and their VH and VL genes were sequenced. The evolution of the plasma antibody responses to all three immunogens was also evaluated. The titers and epitope specificities of autologous and heterologous plasma antibodies elicited by all three immunogens remained stable over the 6-week observation period (Figures S2A—S2C). That is: (1) 426c Core generated autologous, anti-eOD-GT8 and anti-426cOD plasma antibodies (the heterologous antibody responses being exclusively directed to the CD4-bs); (2) eOD-GT8 generated autologous but not heterologous antibodies; and (3) 426cOD elicited strong autologous and anti-eOD-GT8 antibody responses, but weaker anti-426c Core antibody responses (a fraction of the heterologous antibody responses being exclusively directed to the CD4-bs).

Significantly more amino acid mutations accumulated in both the VH and VL genes 6 weeks post-immunization, irrespective of the immunogen (Figures S2D and S2E; Table S5). The H35N mutation was present in 90% of VRC01^{glHC} sequences from 426c Core-immunized animals. Additional mutations were also selected in CDRH1, CDRH2 and FW3 of the VH gene (Table S5B). The H35N mutation was also preferentially selected (71%) in the VRC01^{glHC} sequences from 426cOD-immunized animals (Table S5C). In contrast, no clear pattern of amino acid selection was evident in the VRC01^{glHC} sequences from eOD-GT8 immunized animals (Table S5A).

All VRC01^{glHC}-associated mLCs from the 426c Core-immunized animals were derived from κ8-30*1, and all expressed the 5 amino acid CDRL3 QQY**YK** sequence (i.e., the E96 mutation was not evident) (Table S5B). This sequence also dominated (64%) the mLCs sequences from the 426cOD-immunized animals (Table S5C). The mLC mutations were primarily confined to the CDRL1s and resulted in the accumulation of negatively charged amino acids (Asp or Glu). A more complex pattern of mLCs with 5 AA CDRL3 paired with VRC01^{glHC} was observed in the eOD-GT8-immunized animals (Table S5A). Between weeks 2 and 6 post-immunization, the relative frequency of κ8-30*01 mLCs decreased by approximately half (from 89% to 47%) while the relative frequencies of non-κ8-30*01 mLCs increased by approximately five-fold (from 11% to 53%). While the κ8-30*01 mLCs isolated from the 426c Core-immunized animals were mutated from germline (Table S5B), the majority of κ8-30*01 sequences isolated from the eOD-GT8-immunized animals remained unmutated (15/28 sequences had 0 amino acid mutations) (Table S5A). In contrast, the non-κ8-30 mLCs isolated from eOD-GT8-immunized animals were extensively mutated at week 6 (up to 9 amino acid mutations).

Of note, all the non-κ8-30*01 mLCs have short CDRL1 domains, as is the case of all known VRC01-class bNAbs (Zhou et al., 2013). As observed at week 2 post-immunization, eOD-GT8 preferentially selected for QQY**YT**, QQY**WT** CDRL3s for all κ8-30*01 mLCs but in the case of κ4-61*01, the QQY**ET** sequence was present in 5 of 6 mLCs sequenced and paired with VRC01^{glHC}. The 426cOD selection pattern was intermediate to those of 426c Core as most of the κ8-30*01-associated 5 amino acid CDRL3s expressed the QQY**YK** sequence and the non-κ8-30*01 mLCs were unmutated from germline (Table S5C).

VRC01-like mAbs were generated from paired VH and VL sequences isolated at week 6 from the eOD-GT8-immunized animals, and their binding to the three immunogens were evaluated (Figure 6). We included both κ8-30*01-derived and non-κ8-30*01-derived mAbs, some of which (κ4-61*01) expressed CDRL3s with the QQY**ET** sequence that predominates in the 426c Core-elicited VRC01-like antibody responses (Table S5). None bound the 426c Core and 426cOD proteins. Thus, the presence of shorter CDRL1s on VRC01-like antibodies with κ4-61*01 LCs (5 amino acid CDRL3) does not appear to improve their binding to the VRC01 epitope on heterologous Envs. We expect, however, that VRC01-like BCRs with short CDRL1s can more easily mature toward broadly neutralizing forms, as short CDRL1s are necessary to accommodate the N276 glycans and elements of the V5 gp120 domains (Zhou et al., 2013).

Interactions of Human VRC01-like Antibodies with gl-Targeting Immunogens

We generated VRC01-like antibodies from previously published VH and VL paired sequences from naive human B cells sorted with eOD-GT8 (Havenar-Daughton et al., 2018) and examined their binding to the three "gl-targeting" immunogens (Figure 7; Table S5D). The antibodies only bound eOD-GT8. These results confirm preferential interaction of eOD-GT8-selected VRC01-like antibodies for eOD-GT8 and suggest that the three antigens evaluated here are not recognized by all available variations of human VRC01-like putative antibodies precursors.

DISCUSSION

The development of VRC01-class bnAbs by vaccination will require the activation of their unmutated BCR precursors

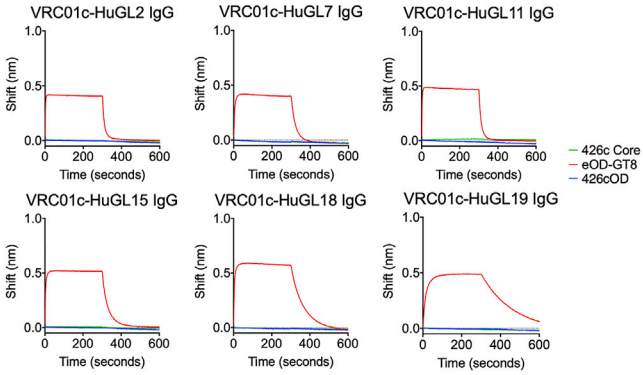

Figure 7. Binding Properties of Human Germline VRC01-like Antibodies Isolated with eOD-GT8, Related to Table S5

Six germline VRC01 antibodies derived from naive human B cells that were sorted by eOD-GT8 were tested for binding against 426c Core, eOD-GT8 or 426cOD using BLI. BLI binding curves are shown. Data representative of 2 independent experiments.

by immunizing with gl-targeting immunogens, and the accumulation of specific VH and VL amino acid mutations through sequential immunizations with heterologous Envs (Dosenovic et al., 2015). Although eOD-GT8 and 426c Core gl-targeting immunogens activate VRC01 precursor B cells *in vivo*, "boost' immunogens that will guide the maturation of VRC01 antibodies toward their broad neutralizing forms have not been identified (Briney et al., 2016; Dosenovic et al., 2015; Parks et al., 2019; Tian et al., 2016). Our study revealed that depending on the background onto which the VRC01 epitope is expressed on the gl-targeting immunogen, B cells with different epitope-specific VH and VL pairs were selected to enter the germinal center reactions. That is, from the available pool of VRC01-like B cells available, each gl-targeting immunogen selected a different subpopulation (containing B cells with different affinities toward that immunogen). As a result, the VRC01 antibody responses elicited by different gl-targeting immunogens displayed distinct heterologous Env cross-recognition properties. We defined a set of mutations responsible for these cross-recognition properties confirming that our studies unveiled differences in the subpopulations of antibodies elicited by different immunogens. We expect therefore that following eOD-GT8 and 426c Core human immunizations, different booster immunogens will be required to further expand the initial waves of VRC01-like B cells stimulated by these two fl-targeting immunogens. Indeed, the VRC01-like antibodies elicited in this animal model by 426c Core are boosted by HxB2 WT Core (Parks et al., 2019), while those elicited by eOD-GT8 expand following a boost immunization with BG505 core-GT3 (Briney et al., 2016). Our data therefore reveal aspects of immunogen-BCR interactions that may have been underappreciated previously, but which we believe will contribute to the development of more effective prime-boost immunization protocols for the elicitation of bnAbs. Our results also highlight potential limitations of eOD-GT8 and 426c Core. eOD-GT8 may not stimulate VRC01 B cells that can bypass the N276 associated glycans, thus necessitating the use of booster immunogens also lacking the N276 glycan site and consequently further increasing the affinities of antibodies that cannot overcome this key obstacle, while 426c Core may activate VRC01 antibodies with long CDRL1 domains that will be less amenable to maturation toward their broadly neutralizing forms.

The observations reported here are applicable to gl-targeting immunogens against other classes of CD4-bs bnAbs (Bonsignori et al., 2016; Williams et al., 2017) and bnAbs against other Env regions such as the apex domain of the HIV-1 trimer (Andrabi et al., 2015), or the N322 glycan patch (Escolano et al., 2019; Steichen et al., 2019), but also to non-HIV bnAbs such as influenza and HCV (Chen et al., 2019; Sangesland et al., 2019).

Subsequent to the initial glVRC01 BCR-selection by germline-targeting immunogens, the fate of the corresponding B cells was defined by the relative affinities of the BCR variants, as others have reported in studies conducted with model antigens (Dal Porto et al., 2002; Kouskoff et al., 1998; Silva et al., 2017). The relative numbers of the high-affinity, epitope-specific glVRC01^{HC}/κ8-30*01 B cells that were preferentially selected by eOD-GT8 and that predominated the early B cell response, decreased over the 6-week period of observation, and their BCRs did not accumulate somatic hypermutations. During the same period, the frequencies of lower affinity VRC01-like B cells expressing different LCs (also paired with glVRC01^{HC}) increased and their BCRs accumulated somatic hypermutations. In contrast, epitope-specific glVRC01^{HC}/κ8-30*01 B cell variants selected by 426c Core had lower affinity for the VRC01 epitope and predominated both during the early and late B cell response and undergone somatic hypermutation.

Overall, our study indicates that the development of effective gl-targeting immunogens to target specific BCRs, such as those known to give rise to bnAbs, will require a better understanding of how the biophysical properties of the epitope and its surrounding surface on the immunogen influences its interaction with the available BCR variants *in vivo*, as structural information or affinity of the immunogen alone are insufficient to accurately predict which BCRs will initially be selected.

Limitations of the Study

Orthologs of the human VH1-2*02 gene are not expressed in animal species such as mice, rats, rabbits, and non-human primates. Thus, the study was conducted in transgenic mice expressing the pre-arranged V, D, and J segment of the inferred germline VRC01 antibody. We expect that the differential selection of VRC01-like antibody subpopulations by the germline-targeting immunogens tested here will be even more pronounced in humans or transgenic animals expressing broader VRC01-class B cell receptors.

STAR★METHODS

Detailed methods are provided in the online version of this paper and include the following:

- KEY RESOURCES TABLE
- RESOURCE AVAILABILITY
  - Lead Contact
  - Materials Availability
  - Data and Code Availability

- EXPERIMENTAL MODEL AND SUBJECT DETAILS
- METHODS DETAILS
  - Computational design of the clade C 426c outer domain
  - Construction of the clade C 426c outer domain
  - Construction of yeast library
  - Yeast display
  - Protein expression and purification
  - Crystallization, data collection and refinement
  - Negative-stain EM sample preparation
  - Negative-Stain EM data collection and processing
  - Biolayer interferometry (BLI)
  - Plasma and antibody ELISA
  - Single cell sorting
  - VH and VL amplification and sequencing
  - Monoclonal antibody production
- QUANTIFICATION AND STATISTICAL ANALYSIS

SUPPLEMENTAL INFORMATION

Supplemental Information can be found online at https://doi.org/10.1016/j.immuni.2020.09.007.

ACKNOWLEDGMENTS

This study was supported by NIH/NIAID grants R01 AI104384 and P01 AI138212. X-ray diffraction data were collected at the Berkeley Center for Structural Biology beamline 5.0.1, which is supported in part by the National Institute of General Medical Sciences. The Advanced Light Source is supported by the Director, Office of Science, Office of Basic Energy Sciences of the United States Department of Energy under contract DE-AC02-05CH11231. P.-S.H. is supported by the United States Department of Energy, Office of Science, Office of Advanced Scientific Computing Research, Scientific Discovery through Advanced Computing (SciDAC) program and Stanford's Bio-X Interdisciplinary Initiatives Seed Grants Program. We thank the James B. Pendleton Charitable Trust for the support of the Formulatrix robotic instrumentation. We would also like to thank Cassie Brian from the Baker lab at the University of Washington for her help with the yeast display experiments.

AUTHOR CONTRIBUTIONS

Conceptualization, L.S., M.P., and P.-S.H.; Methodology, L.S., M.P., P.-S.H., Y.-R.L., and K.R.P.; Investigation, Y.-R.L., K.R.P., C.W., A.S.N., A.K., A.O.R., B.T., J.-H.C., A.J.B., A.S., P.A., and M.G.; Writing, L.S, M.P., P.-S.H., Y.-R.L., K.R.P., and A.S.N.; Funding Acquisition, L.S.; Resources, L.S., M.P., P.-S.H., and D.V.; Supervision, L.S., M.P., and P.-S.H.

DECLARATION OF INTERESTS

The authors declare no competing financial interests. P.-S.H. is an inventor on the patent for eOD (US Patent 10,421,789). L.S. is an inventor on US Patent US 2018/0117140.

Received: March 20, 2020
Revised: June 12, 2020
Accepted: September 10, 2020
Published: October 13, 2020

REFERENCES

Abbott, R.K., Lee, J.H., Menis, S., Skog, P., Rossi, M., Ota, T., Kulp, D.W., Bhullar, D., Kalyuzhniy, O., Havenar-Daughton, C., et al. (2018). Precursor Frequency and Affinity Determine B Cell Competitive Fitness in Germinal Centers, Tested with Germline-Targeting HIV Vaccine Immunogens. Immunity *48*, 133–146.

Adams, P.D., Afonine, P.V., Bunkóczi, G., Chen, V.B., Davis, I.W., Echols, N., Headd, J.J., Hung, L.W., Kapral, G.J., Grosse-Kunstleve, R.W., et al. (2010). PHENIX: a comprehensive Python-based system for macromolecular structure solution. Acta Crystallogr. D Biol. Crystallogr. *66*, 213–221.

Afonine, P.V., Grosse-Kunstleve, R.W., Echols, N., Headd, J.J., Moriarty, N.W., Mustyakimov, M., Terwilliger, T.C., Urzhumtsev, A., Zwart, P.H., and Adams, P.D. (2012). Towards automated crystallographic structure refinement with phenix.refine. Acta Crystallogr. D Biol. Crystallogr. *68*, 352–367.

Andrabi, R., Voss, J.E., Liang, C.H., Briney, B., McCoy, L.E., Wu, C.Y., Wong, C.H., Poignard, P., and Burton, D.R. (2015). Identification of Common Features in Prototype Broadly Neutralizing Antibodies to HIV Envelope V2 Apex to Facilitate Vaccine Design. Immunity *43*, 959–973.

Bonsignori, M., Zhou, T., Sheng, Z., Chen, L., Gao, F., Joyce, M.G., Ozorowski, G., Chuang, G.Y., Schramm, C.A., Wiehe, K., et al.; NISC Comparative Sequencing Program (2016). Maturation Pathway from Germline to Broad HIV-1 Neutralizer of a CD4-Mimic Antibody. Cell *165*, 449–463.

Borst, A.J., Weidle, C.E., Gray, M.D., Frenz, B., Snijder, J., Joyce, M.G., Georgiev, I.S., Stewart-Jones, G.B., Kwong, P.D., McGuire, A.T., et al. (2018). Germline VRC01 antibody recognition of a modified clade C HIV-1 envelope trimer and a glycosylated HIV-1 gp120 core. eLife *7*, e37688.

Briney, B., Sok, D., Jardine, J.G., Kulp, D.W., Skog, P., Menis, S., Jacak, R., Kalyuzhniy, O., de Val, N., Sesterhenn, F., et al. (2016). Tailored Immunogens Direct Affinity Maturation toward HIV Neutralizing Antibodies. Cell *166*, 1459–1470.

Brochet, X., Lefranc, M.P., and Giudicelli, V. (2008). IMGT/V-QUEST: the highly customized and integrated system for IG and TR standardized V-J and V-D-J sequence analysis. Nucleic Acids Res. *36*, W503-8.

Burton, D.R., and Hangartner, L. (2016). Broadly Neutralizing Antibodies to HIV and Their Role in Vaccine Design. Annu. Rev. Immunol. *34*, 635–659.

Charif, D., and Lobry, J.R. (2007). SeqinR 1.0–2: a contributed package to the R Project for statistical computing devoted to biological sequences retrieval and analysis. In Structural Approaches to Sequence Evolution: Molecules, Networks, Populations, U. Bastolla, M. Porto, E. Roman, and M. Vendruscolo, eds. (Springer), pp. 207–232.

Chen, F., Tzarum, N., Wilson, I.A., and Law, M. (2019). V_H1-69 antiviral broadly neutralizing antibodies: genetics, structures, and relevance to rational vaccine design. Curr. Opin. Virol. *34*, 149–159.

Crooks, G.E., Hon, G., Chandonia, J.M., and Brenner, S.E. (2004). WebLogo: a sequence logo generator. Genome Res. *14*, 1188–1190.

Dal Porto, J.M., Haberman, A.M., Kelsoe, G., and Shlomchik, M.J. (2002). Very low affinity B cells form germinal centers, become memory B cells, and participate in secondary immune responses when higher affinity competition is reduced. J. Exp. Med. *195*, 1215–1221.

Dosenovic, P., von Boehmer, L., Escolano, A., Jardine, J., Freund, N.T., Gitlin, A.D., McGuire, A.T., Kulp, D.W., Oliveira, T., Scharf, L., et al. (2015). Immunization for HIV-1 Broadly Neutralizing Antibodies in Human Ig Knockin Mice. Cell *161*, 1505–1515.

Emsley, P., and Cowtan, K. (2004). Coot: model-building tools for molecular graphics. Acta Crystallogr. D Biol. Crystallogr. *60*, 2126–2132.

Emsley, P., Lohkamp, B., Scott, W.G., and Cowtan, K. (2010). Features and development of Coot. Acta Crystallogr D Biol Crystallogr. *66*, 486–501.

Escolano, A., Gristick, H.B., Abernathy, M.E., Merkenschlager, J., Gautam, R., Oliveira, T.Y., Pai, J., West, A.P., Jr., Barnes, C.O., Cohen, A.A., et al. (2019). Immunization expands B cells specific to HIV-1 V3 glycan in mice and macaques. Nature *570*, 468–473.

Giudicelli, V., Brochet, X., and Lefranc, M.-P. (2011). IMGT/V-QUEST: IMGT standardized analysis of the immunoglobulin (IG) and T cell receptor (TR) nucleotide sequences. Cold Spring Harb. Protoc. *2011*, 695–715.

Havenar-Daughton, C., Sarkar, A., Kulp, D.W., Toy, L., Hu, X., Deresa, I., Kalyuzhniy, O., Kaushik, K., Upadhyay, A.A., Menis, S., et al. (2018). The human naive B cell repertoire contains distinct subclasses for a germline-targeting HIV-1 vaccine immunogen. Sci. Transl. Med. *10*, eaat0381.

Hofmeyer, T., Schmelz, S., Degiacomi, M.T., Dal Peraro, M., Daneschdar, M., Scrima, A., van den Heuvel, J., Heinz, D.W., and Kolmar, H. (2013). Arranged

sevenfold: structural insights into the C-terminal oligomerization domain of human C4b-binding protein. J. Mol. Biol. *425*, 1302–1317.

Huang, P.S., Ban, Y.E., Richter, F., Andre, I., Vernon, R., Schief, W.R., and Baker, D.; RosettaRemodel (2011). RosettaRemodel: a generalized framework for flexible backbone protein design. PLoS ONE *6*, e24109.

Huang, J., Kang, B.H., Ishida, E., Zhou, T., Griesman, T., Sheng, Z., Wu, F., Doria-Rose, N.A., Zhang, B., McKee, K., et al. (2016). Identification of a CD4-Binding-Site Antibody to HIV that Evolved Near-Pan Neutralization Breadth. Immunity *45*, 1108–1121.

Jardine, J., Julien, J.P., Menis, S., Ota, T., Kalyuzhniy, O., McGuire, A., Sok, D., Huang, P.S., MacPherson, S., Jones, M., et al. (2013). Rational HIV immunogen design to target specific germline B cell receptors. Science *340*, 711–716.

Jardine, J.G., Ota, T., Sok, D., Pauthner, M., Kulp, D.W., Kalyuzhniy, O., Skog, P.D., Thinnes, T.C., Bhullar, D., Briney, B., et al. (2015). HIV-1 VACCINES. Priming a broadly neutralizing antibody response to HIV-1 using a germline-targeting immunogen. Science *349*, 156–161.

Jardine, J.G., Kulp, D.W., Havenar-Daughton, C., Sarkar, A., Briney, B., Sok, D., Sesterhenn, F., Ereño-Orbea, J., Kalyuzhniy, O., Deresa, I., et al. (2016). HIV-1 broadly neutralizing antibody precursor B cells revealed by germline-targeting immunogen. Science *351*, 1458–1463.

Kimanius, D., Forsberg, B.O., Scheres, S.H., and Lindahl, E. (2016). Accelerated cryo-EM structure determination with parallelisation using GPUs in RELION-2. eLife *5*, e18722.

Kouskoff, V., Famiglietti, S., Lacaud, G., Lang, P., Rider, J.E., Kay, B.K., Cambier, J.C., and Nemazee, D. (1998). Antigens varying in affinity for the B cell receptor induce differential B lymphocyte responses. J. Exp. Med. *188*, 1453–1464.

Kwong, P.D., and Mascola, J.R. (2012). Human antibodies that neutralize HIV-1: identification, structures, and B cell ontogenies. Immunity *37*, 412–425.

Lander, G.C., Stagg, S.M., Voss, N.R., Cheng, A., Fellmann, D., Pulokas, J., Yoshioka, C., Irving, C., Mulder, A., Lau, P.W., et al. (2009). Appion: an integrated, database-driven pipeline to facilitate EM image processing. J. Struct. Biol. *166*, 95–102.

Ludtke, S.J., Baldwin, P.R., and Chiu, W. (1999). EMAN: semiautomated software for high-resolution single-particle reconstructions. J. Struct. Biol. *128*, 82–97.

McCoy, L.E., and Burton, D.R. (2017). Identification and specificity of broadly neutralizing antibodies against HIV. Immunol. Rev. *275*, 11–20.

McCoy, A.J., Grosse-Kunstleve, R.W., Adams, P.D., Winn, M.D., Storoni, L.C., and Read, R.J. (2007). Phaser crystallographic software. J. Appl. Cryst. *40*, 658–674.

McGuire, A.T., Gray, M.D., Dosenovic, P., Gitlin, A.D., Freund, N.T., Petersen, J., Correnti, C., Johnsen, W., Kegel, R., Stuart, A.B., et al. (2016). Specifically modified Env immunogens activate B-cell precursors of broadly neutralizing HIV-1 antibodies in transgenic mice. Nat. Commun. *7*, 10618.

Medina-Ramírez, M., Garces, F., Escolano, A., Skog, P., de Taeye, S.W., Del Moral-Sanchez, I., McGuire, A.T., Yasmeen, A., Behrens, A.J., Ozorowski, G., et al. (2017). Design and crystal structure of a native-like HIV-1 envelope trimer that engages multiple broadly neutralizing antibody precursors in vivo. J. Exp. Med. *214*, 2573–2590.

Mindell, J.A., and Grigorieff, N. (2003). Accurate determination of local defocus and specimen tilt in electron microscopy. J. Struct. Biol. *142*, 334–347.

Mouquet, H., Scheid, J.F., Zoller, M.J., Krogsgaard, M., Ott, R.G., Shukair, S., Artyomov, M.N., Pietzsch, J., Connors, M., Pereyra, F., et al. (2010). Polyreactivity increases the apparent affinity of anti-HIV antibodies by heteroligation. Nature *467*, 591–595.

Otwinowski, Z., and Minor, W. (1997). Processing of X-ray diffraction data collected in oscillation mode. Methods Enzymol. *276*, 307–326.

Pages, H., Aboyoun, P., Gentleman, R., and DebRoy, S. (2018). Biostrings: efficient manipulation of biological strings. http://bioconductor.org/packages/release/bioc/html/Biostrings.html.

Parks, K.R., MacCamy, A.J., Trichka, J., Gray, M., Weidle, C., Borst, A.J., Khechaduri, A., Takushi, B., Agrawal, P., Guenaga, J., et al. (2019). Overcoming Steric Restrictions of VRC01 HIV-1 Neutralizing Antibodies through Immunization. Cell Rep. *29*, 3060–3072.

Pejchal, R., Doores, K.J., Walker, L.M., Khayat, R., Huang, P.S., Wang, S.K., Stanfield, R.L., Julien, J.P., Ramos, A., Crispin, M., et al. (2011). A potent and broad neutralizing antibody recognizes and penetrates the HIV glycan shield. Science *334*, 1097–1103.

R Core Team (2018). R: The R Project for Statistical Computing. https://www.R-project.org/.

Sajadi, M.M., Dashti, A., Rikhtegaran Tehrani, Z., Tolbert, W.D., Seaman, M.S., Ouyang, X., Gohain, N., Pazgier, M., Kim, D., Cavet, G., et al. (2018). Identification of Near-Pan-neutralizing Antibodies against HIV-1 by Deconvolution of Plasma Humoral Responses. Cell *173*, 1783–1795.

Sangesland, M., Ronsard, L., Kazer, S.W., Bals, J., Boyoglu-Barnum, S., Yousif, A.S., Barnes, R., Feldman, J., Quirindongo-Crespo, M., McTamney, P.M., et al. (2019). Germline-Encoded Affinity for Cognate Antigen Enables Vaccine Amplification of a Human Broadly Neutralizing Response against Influenza Virus. Immunity. *51*, 735–749.

Scharf, L., West, A.P., Sievers, S.A., Chen, C., Jiang, S., Gao, H., Gray, M.D., McGuire, A.T., Scheid, J.F., Nussenzweig, M.C., et al. (2016). Structural basis for germline antibody recognition of HIV-1 immunogens. eLife *5*, e13783.

Scheid, J.F., Mouquet, H., Feldhahn, N., Walker, B.D., Pereyra, F., Cutrell, E., Seaman, M.S., Mascola, J.R., Wyatt, R.T., Wardemann, H., and Nussenzweig, M.C. (2009). A method for identification of HIV gp140 binding memory B cells in human blood. J. Immunol. Methods *343*, 65–67.

Scheid, J.F., Mouquet, H., Ueberheide, B., Diskin, R., Klein, F., Oliveira, T.Y., Pietzsch, J., Fenyo, D., Abadir, A., Velinzon, K., et al. (2011). Sequence and structural convergence of broad and potent HIV antibodies that mimic CD4 binding. Science *333*, 1633–1637.

Scheres, S.H. (2012). A Bayesian view on cryo-EM structure determination. J. Mol. Biol. *415*, 406–418.

Scheres, S.H., and Chen, S. (2012). Prevention of overfitting in cryo-EM structure determination. Nat. Methods *9*, 853–854.

Shih, T.A., Meffre, E., Roederer, M., and Nussenzweig, M.C. (2002). Role of BCR affinity in T cell dependent antibody responses in vivo. Nat. Immunol. *3*, 570–575.

Silva, M., Nguyen, T.H., Philbrook, P., Chu, M., Sears, O., Hatfield, S., Abbott, R.K., Kelsoe, G., and Sitkovsky, M.V. (2017). Targeted Elimination of Immunodominant B Cells Drives the Germinal Center Reaction toward Subdominant Epitopes. Cell Rep. *21*, 3672–3680.

Snijder, J., Ortego, M.S., Weidle, C., Stuart, A.B., Gray, M.D., McElrath, M.J., Pancera, M., Veesler, D., and McGuire, A.T. (2018). An Antibody Targeting the Fusion Machinery Neutralizes Dual-Tropic Infection and Defines a Site of Vulnerability on Epstein-Barr Virus. Immunity. *48*, 799–811.

Steichen, J.M., Lin, Y.C., Havenar-Daughton, C., Pecetta, S., Ozorowski, G., Willis, J.R., Toy, L., Sok, D., Liguori, A., Kratochvil, S., et al. (2019). A generalized HIV vaccine design strategy for priming of broadly neutralizing antibody responses. Science *366*, eaax4380.

Suloway, C., Pulokas, J., Fellmann, D., Cheng, A., Guerra, F., Quispe, J., Stagg, S., Potter, C.S., and Carragher, B. (2005). Automated molecular microscopy: the new Leginon system. J. Struct. Biol. *151*, 41–60.

Tas, J.M., Mesin, L., Pasqual, G., Targ, S., Jacobsen, J.T., Mano, Y.M., Chen, C.S., Weill, J.C., Reynaud, C.A., Browne, E.P., et al. (2016). Visualizing antibody affinity maturation in germinal centers. Science *351*, 1048–1054.

Tian, M., Cheng, C., Chen, X., Duan, H., Cheng, H.L., Dao, M., Sheng, Z., Kimble, M., Wang, L., Lin, S., et al. (2016). Induction of HIV Neutralizing Antibody Lineages in Mice with Diverse Precursor Repertoires. Cell. *166*, 1471–1484.

Tiller, T., Busse, C.E., and Wardemann, H. (2009). Cloning and expression of murine Ig genes from single B cells. J. Immunol. Methods *350*, 183–193.

Umotoy, J., Bagaya, B.S., Joyce, C., Schiffner, T., Menis, S., Saye-Francisco, K.L., Biddle, T., Mohan, S., Vollbrecht, T., Kalyuzhniy, O., et al. (2019). Rapid and Focused Maturation of a VRC01-Class HIV Broadly Neutralizing Antibody Lineage Involves Both Binding and Accommodation of the N276-Glycan. Immunity. *51*, 141–154.

Veesler, D., Cupelli, K., Burger, M., Gräber, P., Stehle, T., and Johnson, J.E. (2014). Single-particle EM reveals plasticity of interactions between the adenovirus penton base and integrin αVβ3. Proc Natl Acad Sci USA. *111*, 8815–8819.

Victora, G.D., and Nussenzweig, M.C. (2012). Germinal centers. Annu. Rev. Immunol. *30*, 429–457.

Voss, N.R., Yoshioka, C.K., Radermacher, M., Potter, C.S., and Carragher, B. (2009). DoG Picker and TiltPicker: software tools to facilitate particle selection in single particle electron microscopy. J Struct Biol. *166*, 205–213.

West, A.P., Jr., Diskin, R., Nussenzweig, M.C., and Bjorkman, P.J. (2012). Structural basis for germ-line gene usage of a potent class of antibodies targeting the CD4-binding site of HIV-1 gp120. Proc. Natl. Acad. Sci. USA *109*, E2083–E2090.

Wickham, H. (2017). Tidyverse: easily install and load the "tidyverse.". https://cran.r-project.org/web/packages/tidyverse/index.html.

Williams, W.B., Zhang, J., Jiang, C., Nicely, N.I., Fera, D., Luo, K., Moody, M.A., Liao, H.X., Alam, S.M., Kepler, T.B., et al. (2017). Initiation of HIV neutralizing B cell lineages with sequential envelope immunizations. Nat. Commun. *8*, 1732.

Zhou, T., Georgiev, I., Wu, X., Yang, Z.Y., Dai, K., Finzi, A., Kwon, Y.D., Scheid, J.F., Shi, W., Xu, L., et al. (2010). Structural basis for broad and potent neutralization of HIV-1 by antibody VRC01. Science *329*, 811–817.

Zhou, T., Zhu, J., Wu, X., Moquin, S., Zhang, B., Acharya, P., Georgiev, I.S., Altae-Tran, H.R., Chuang, G.Y., Joyce, M.G., et al.; NISC Comparative Sequencing Program (2013). Multidonor analysis reveals structural elements, genetic determinants, and maturation pathway for HIV-1 neutralization by VRC01-class antibodies. Immunity *39*, 245–258.

Zivanov, J., Nakane, T., Forsberg, B.O., Kimanius, D., Hagen, W.J., Lindahl, E., and Scheres, S.H. (2018). New tools for automated high-resolution cryo-EM structure determination in RELION-3. eLife *7*, e42166.

STAR★METHODS

KEY RESOURCES TABLE

REAGENT or RESOURCE	SOURCE	IDENTIFIER
Antibodies		
FITC Rat Anti-Mouse IgG1 (clone A85-1)	BD Biosciences	Cat# 553443; RRID: AB_394862
FITC Rat Anti-Mouse IgG2b (clone R12-3)	BD Biosciences	Cat# 553395; RRID: AB_394833
Goat anti Mouse IgG2c:FITC	Bio-Rad	Cat# STAR135F; RRID: AB_1102667
FITC Rat Anti-Mouse IgG3 (clone R40-82)	BD Biosciences	Cat# 553403; RRID: AB_394840
PerCP/Cy5.5 anti-mouse IgD Antibody	Biolegend	Cat# 405710; RRID: AB_1575113
eBioscience Fixable Viability Dye eFluor 506	ThermoFisher Scientific	Cat# 65-0866-14
BV510 Hamster Anti-Mouse CD3e (clone 145-2c11)	BD Biosciences	Cat# 563024; RRID: AB_2737959
BV510 Rat Anti-Mouse CD4 (clone RM4-5)	BD Biosciences	Cat# 563106; RRID: AB_2687550
BV 510 Rat Anti-Mouse Ly-6G and Ly6C (clone RB6-8C5)	BD Biosciences	Cat# 563040; RRID: AB_2722496
Brilliant Violent 510 anti-mouse F4/80 Antibody	Biolegend	Cat# 123135; RRID: AB_2562622
Brilliant Violet 605 anti-mouse IgM Antibody	Biolegend	Cat# 406523; RRID: AB_2563358
BV786 Rat Anti-Mouse CD45R/B220	BD Bioscience	Cat# 563894; RRID: AB_2738472
BV650 Rat Anti-Mouse CD19	BD Biosciences	Cat# 563235; RRID: AB_2738085
6x-His Tag Monoclonal Antibody (HIS.H8)	ThermoFisher Scientific	Cat# MA1–21315; RRID: AB_557403
HRP Goat anti-mouse IgG	Biolegend	Cat# 405306; RRID: AB_315009
anti-C-Myc Antibody (Chicken) - FITC Conjugated	Immunology Consultant Lab	Cat# CMYC-45F
Bacterial and Virus Strains		
NEB® 5-alpha Competent *E. coli* (High Efficiency)	New England BioLabs	Cat# C2987H
Chemicals, Peptides, and Recombinant Proteins		
Poly (I:C)	Invivogen	Cat# tlrl-pic-5
GLA-LSQ	Infectious Disease Reseach Institute (IDRI)	Cat# IDRI-LS130
Steptavidin-R-Phycoerythirin	Prozyme	Cat# PJRS25
Streptavidin-Allophycocyanin	Prozyme	Cat# PJ27S
RNaseOUT™ Recombinant Ribonuclease Inhibitor	ThermoFisher Scientific	Cat# 10777019
HotStar Taq Plus	QIAGEN	Cat# 203607
Gel Red Nucleic Acid Stain	Biotium	Cat# 41002
ExoSap-IT	Affymetrix	Cat# 78201
Endoproteinase LysC	New England BioLabs	Cat# P8109S
SureBlue Reserve TMB Microwell Peroxidase Substrate	KPL	Cat# 53-00-02
293-Free Transfection Reagent	Millipore Sigma	Cat# 72181
5x In-Fusion enzyme	Takara Bio	Cat# 1805251A
SuperScript IV RT	ThermoFisher Scientific	Cat# 18090200
Critical Commercial Assays		
InFusion HD Cloning Kit	Takara Bio	Cat# 639649
QIAprep Spin Miniprep Kit	QIAGEN	Cat# 27106
GeneMorph II Random Mutagenesis Kit	Agilent	Cat# 200550
EZ-Link™ NHS-PEG4-Biotin	ThermoFisher Scientific	Cat# 21362

(*Continued on next page*)

Continued

REAGENT or RESOURCE	SOURCE	IDENTIFIER
QuikChange II Site-Directed Mutagenesis Kit	Agilent	Cat# 200523
QIAquick Gel Extraction Kit	QIAGEN	Cat# 28704
Deposited Data		
VRC01 Fab + 426cOD crystal structure	This paper	Protein Data Bank, PBD: 6VLW
Antibody sequences	This paper	GenBank, Accession numbers: MT585207-MT585272
426cOD	This paper	GenBank Accession number: MT671449
Experimental Models: Organisms/Strains		
Mouse: glH-VRC01	Jardine et al., 2015	N/A
Oligonucleotides		
Random Primers	ThermoFisher Scientific	Cat# 48190011
GeneAmp dNTP Blend	ThermoFisher Scientific	Cat# N8080261
Primers for PCR	Parks et al., 2019; Jardine et al., 2015; Tiller et al., 2009	N/A
Recombinant DNA		
Ptt3 k vector	Snijder et al., 2018	N/A
PMN 4-341 vector	Mouquet et al., 2010	N/A
pETcon(-) plasmid	Addgene, Andrew Scharenberg	Plasmid #41522; RRID: Addgene_41522; http://n2t.net/addgene/41522
Software and Algorithms		
Coot	Emsley et al., 2010	https://www2.mrc-lmb.cam.ac.uk/personal/pemsley/coot/
HKL-2000	Otwinowski and Minor, 1997	https://hkl-xray.com/download-instructions-hkl-2000
RosettaRemodel	Huang et al., 2011	https://www.rosettacommons.org/docs/latest/application_documentation/design/rosettaremodel
Leginon	Suloway et al., 2005	https://emg.nysbc.org/redmine/projects/leginon/wiki/Leginon_Homepage
RELION/3.0	Zivanov et al., 2018; Kimanius et al., 2016; Scheres, 2012; Scheres and Chen, 2012	N/A
EMAN 1.9	Ludtke et al., 1999	https://blake.bcm.edu/emanwiki/EMAN1
Appion	Lander et al., 2009	N/A
CTFFIND4	Mindell and Grigorieff, 2003	https://grigoriefflab.umassmed.edu/ctf_estimation_ctffind_ctftilt
Pymol	Schrödinger	https://pymol.org/2/
Phenix.refine	Afonine et al., 2012	N/A
Phaser	McCoy et al., 2007	N/A
Geneious (Version 8.1.9)	Biomatters Ltd.	https://www.geneious.com
R (Version 3.4.1)	R Core Team, 2018	https://www.R-project.org/
IMGT/V-QUEST	Brochet et al., 2008; Giudicelli et al., 2011	http://www.imgt.org/IMGT_vquest/input
Tidyverse	Wickham, 2017	https://cran.r-project.org/web/packages/tidyverse/index.html
Biostrings	Pages et al., 2018	http://bioconductor.org/packages/release/bioc/html/Biostrings.html
Prism 7	GraphPad	https://www.graphpad.com
seqinr	Charif and Lobry, 2007	N/A

(*Continued on next page*)

Continued

REAGENT or RESOURCE	SOURCE	IDENTIFIER
Other		
Anti-PE microbeads	Miltenyi Biotech	Cat# 130-048-801
Anti-APC microbeads	Miltenyi Biotech	Cat# 130-090-855
LS Columns	Miltenyi Biotech	Cat# 130-042-401
Pierce Protein A agarose beads	ThermoFisher Scientific	Cat# 20334
Anti-human IgG Fc Capture (AHC) Biosensors	ForteBio	Cat# 18-5063
Anti-Human Fab-CH1 2nd Generation (FAB2G) Biosensors	ForteBio	Cat# 18-5126
His60 Ni-Superflow Resin	Takara Bio	Cat# 636660
HiLoad 16/600 Superdex 200 pg (GE) column	GE Healthcare	Cat# 28989335
Agarose Bound Galanthus Nivalis Lectin	Vector Labs	Cat# AL-1243-5
HisTrap Fast Flow Column	GE Healthcare	Cat# 17525501
Accuprime Pfx Supermix	ThermoFisher Scientific	Cat# 12344040
293F transfection reagent	Millipore Sigma	Cat# 72181

RESOURCE AVAILABILITY

Lead Contact

Further information and requests for reagents should be directed to and will be fulfilled by Leonidas Stamatatos (lstamata@fredhutch.org).

Materials Availability

All reagents generated in this study can be made available upon request through Materials Transfer Agreements.

Data and Code Availability

The accession numbers of the monoclonal antibodies reported here are GenBank: MT585207–MT585272. The monoclonal antibody sequences have also been deposited on the GitHub repository: https://github.com/krparks/epitope_presentation. The accession number for the sequence of 426cOD reported here is GenBank : MT671449. Coordinates and structure factors for 426cOD in complex with mature VRC01 Fab have been deposited with the Protein Data Bank, PDB: 6VLW. Data collection and refinement statistics can be found in Table S2.

EXPERIMENTAL MODEL AND SUBJECT DETAILS

Immunizations were performed with the C4b-based nanoparticles (heptameric forms) (Hofmeyer et al., 2013). Immunizations were performed in the gl_H-VRC01 mouse (Jardine et al., 2015). It is heterozygous for the transgene (glVRC01 HC) and expresses mouse light chains. Details on the number of animals used are presented in Table S6. 6-12 week old glH-VRC01 knock-in mice were immunized intramuscularly with 60 μg or 50 μg of recombinant Env along with 60 μg of polyinosinic:polycytidylic acid (poly (I:C)) or 50 ul GLA-LSQ (IDRI) split between the rear hind legs. Male and female mice were included in this study. Blood was collected via cardiac puncture two- or six-weeks following immunization, at which time spleen and lymph nodes were also harvested. Spleen and lymph nodes were processed into a single cell suspension separately and frozen in FBS + 10% DMSO and stored in liquid nitrogen until further use. Blood, spleens and lymph nodes were also isolated from non-immunized animals. The Fred Hutch Institutional Animal Care and Use Committee approved all mouse studies.

METHODS DETAILS

Computational design of the clade C 426c outer domain

RosettaRemodel (RosettaRemodel: A Generalized Framework for Flexible Backbone Protein Design; https://dx.plos.org/10.1371/journal.pone.0024109) was used to engineer a gp120 outer domain of 426c based on 426c Core (426c TM4Δ1-3) (McGuire et al., 2016). To isolate the outer domain from inner domain, the C terminus of the α5 helix and N terminus of C2 region was closed with RosettaRemodel and a new N and C terminus of the outer domain was introduced before V4. To improve antibody interaction, asparagine(N)-linked glycan groups shielding the CD4-bs, at residues 289_{gp120}, 332_{gp120}, and 391_{gp120}, were mutated to glutamines. A glycan site at position 448_{gp120} was re-introduced to the 426c sequence, as it was previously identified to be kinetically important for

proper folding of the engineered outer domain. RosettaRemodel was used to introduce mutations in the residues adjacent the CD4-bs.

Comparison of the 426c outer domain with eOD identified differences in the position and rigidity of a helix important in CD4 and antibody binding (Figure S3). Therefore, this helix was lengthened by two residues on the C-terminal end to extend it into the binding region and RosettaRemodel's -build_disulf was used to introduce disulfide bonds and lock the helix into the conformation compatible with glVRC01-binsing. The space behind the helix in 426cOD had increased polarity and reduced packing compared to that of eOD (Figure S3B and 3c), which includes many nonpolar and bulky residues in the pocket. Therefore, we replaced the incompatible residues in this region using RosettaRemodel's manual design features. S2, which was among the lowest-energy and most-populated clusters of the resulting models, was selected for further testing (Figure S3D). The sequence of S2 is reported in Table S1, with the mutations from 426c highlighted. S2 was able to bind a subset of mature bnAbs: VRC-PG20, VRC01, and 3BNC60; but not germline ones (Figure S3E and 3F, respectively).

In S2, the helix and the V5 loop were subsequently, brought closer together by extending the helix by one turn, allowing the two structures to better interact (Figure S3E and 3 h). To increase the packing and stability of the helix and V5 loop, we created an extended hydrogen bond network in the space (Figure S3I). As a result, S2 gained the ability to bind a germline VRC01 antibody, glVRC-PG20 (Figure S3K). This binding is dependent upon the residue at position 51 (Figure S3L). In S2 this residue is an aspartic acid which hydrogen bonds with residues in V5, but when it is mutated to an isoleucine such interactions are not there and the protein is not recognized by glVRC-PG20 (Figure S3J).

Construction of the clade C 426c outer domain

We ordered 426cOD-base gene segments with flanking segments homologous to pTT3 vector from Integrated DNA Technologies (IDT). We then used In-Fusion HD Cloning Plus system (Takara Bio USA, Inc.) to clone the gene construct into pTT3 vector with C-terminal 6x His-Avi-Tag.

Construction of yeast library

PCR and sequencing primers were obtained from IDT (Table S7). The 426cOD-base gene segment was amplified using extension primers to add pETcon(-) yeast homologous recombination segments to each end. The GeneMorph II Random Mutagenesis Kit (Agilent) was used to generate the library which was then run on a 1% agarose gel and the gene was gel extracted and purified (QIAGEN QIAquick Gel Extraction Kit). The purified library pool was then amplified with the extension primers to generate 12 μg of DNA. Yeast EBY100 cells were transformed with library DNA and linearized pETcon(-) plasmid (McGuire et al., 2016). After transformation (minimum of 1E7 transformants), cells were grown for two days in SDCAA medium at 30°C. Cells can then be galactose induced with SGCAA media for yeast display experiment or stored in SDCAA with 20% glycerol (w/v) at 1E7 cells per aliquot at −80°C.

Yeast display

Cell aliquots were thawed on ice and centrifuged at 13,000 RPM for 30 s, resuspended at 1E7 cells per ml of C-Trp-Ura medium, and grown at 30°C overnight. Cells were then centrifuged at 13,000 RPM for 1 min and resuspended (1E7 per ml) in SGCAA medium and induced at 30°C for 16-20 h. glVRC01 IgG was biotinylated with EZ-Link NHS-PEG_4-Biotin and labeling kit (Thermo Fisher Scientific) at a one to one ratio of protein to biotin and tetramerized with streptavidin-phycoerythrin. Yeast cells expressing Env on their surface (based on glVRC01-SAPE and anti-c-Myc fluorescein isothiocyanate (FITC, Immunology Consultant Lab) staining) were sorted using a Sony SH800. Sorted cells were grown for two days in C-Trp-Ura media at 30°C. After 4 rounds of sorting the cells were plated on a C-Trp-Ura agarose plate. DNA from individual colonies was isolated and sequenced (GENEWIZ) to identify potential amino acid mutations that lead to glVRC01-recognition. Mutations were then introduced into the mammalian pTT3 426c base plasmid by site-directed mutagenesis using Quick Change II system (Agilent Technologies, Inc.) and conventional primers ordered from IDT (Table S7).

Protein expression and purification

All the recombinant envelopes were expressed and purified as previously described (McGuire et al., 2016; Parks et al., 2019) Briefly, Envs were produced in 293E or 293F. Cell supernatants were purified by lectin affinity chromatography (*Galanthus nivalis*, Vector Labs), then subjected to Superdex 200 size exclusion chromatography (GE Healthcare).

Monomeric proteins were produced by transfecting 293E cells with Env encoding plasmid. Cells are cultured for 6 days at 37°C, 5% CO_2, 80% humidity, and shaking at 125 RPM. Cells were centrifuged for 3000 RPM for 30 min and the supernatant sterile filtered through at 0.22 uM filter. Protein was purified by passing the cellular supernatant over a 5ml HisTrap Fast Flow column. The eluted protein was purified on SEC as described above.

426c Core and 426cOD CD4-bs KO Env constructs contain the D368R, E370A, and D279A mutations, while the eOD-GT8 KO contains the D368R mutation and the amino acids at positions 276-279 have been mutated to "NFTA."

Crystallization, data collection and refinement

The VRC01 Fab and 426cOD complex was formed by mixing equal molar parts of VRC01 Fab and 426cOD for 1 h at room temperature. The complex was concentrated to ~10 mgs/mL for crystallization trials. Crystallization conditions were screened and monitored with an NT8 drop setter and Rock Imager (Formulatrix). Screening was done with Rigaku Wizard Precipitant Synergy block

no. 2, Molecular Dimensions Proplex screen HT-96, and Hampton Research Crystal Screen HT using the sitting drop vapor diffusion method. Final crystals were grown in a solution of 18.43% PEG 3350, 11- 0.01%, Lithium Sulfate, 0.11 M Imidazole pH 6.5. Crystals were cryoprotected in a solution of 30% excess of the crystallization condition and 20% glycerol. Crystals were sent to ALS 5.0.1 and diffraction data was collected to 3.42 Å. Data was processed using HKL-2000 (Otwinowski and Minor, 1997). The structure was solved using molecular replacement using PDB ID: 5IFA as a search model in Phaser in Phenix (Adams et al., 2010). The structure was further refined with COOT (Emsley and Cowtan, 2004) and Phenix (Adams et al., 2010). The refinement statistics are summarized in Table S2.

Negative-stain EM sample preparation

All nanoparticle constructs used in this study (3 μL) were negatively stained at final concentrations between 10 μg/mL and 20 μg/mL using Gilder Grids overlaid with a thin layer of amorphous carbon and 2% uranyl formate, as previously described (Veesler et al., 2014).

Negative-Stain EM data collection and processing

Data were collected on an FEI Technai 12 Spirit 120kV electron microscope equipped with a Gatan Ultrascan 4000 CCD camera. A total of 150-200 images were collected per sample by using a random defocus range of 1.5–2.5 μm with a total exposure of 45 $e-/A^2$. Data were automatically acquired using Leginon (Suloway et al., 2005), and data processing was carried out using Appion (Lander et al., 2009). The parameters of the contrast transfer function (CTF) were estimated using CTFFIND4 (Mindell and Grigorieff, 2003), and particles were picked in a reference-free manner using DoG picker (Voss et al., 2009). Particles were extracted with a binning factor of 2 after correcting for the effect of the CTF by flipping the phases of each micrograph with EMAN 1.9 (Ludtke et al., 1999). Particle stacks were pre-processed in RELION/3.0 (Zivanov et al., 2018; Kimanius et al., 2016; Scheres, 2012; Scheres and Chen, 2012) with an additional binning factor of 2 applied, resulting in a final pixel size of 6.4 Å. Resulting particles were sorted by reference-free 2D classification over 25 iterations.

Biolayer interferometry (BLI)

Antibody binding to recombinant Env proteins was determined using biolayer interferometry on the Octet Red 96 (ForteBio, Inc, Menlo Park, CA). Briefly, anti-human Fc capture biosensors (ForteBio, Cat#: 18-5063) were activated by immersion into 1x Kinetics Buffer (1x PBS, 0.1% BSA, 0.02% Tween-20, 0.005% NaN3) for 10 min. Antibodies were loaded onto an anti-human Fc capture probe at 20 ug/mL. The probes were then dipped into solutions containing 2 uM recombinant Env. Parameters for all BLI assays were: 30 s of baseline measurement, 240 s to load the antibody onto the anti-human Fc capture probe, 60 s of baseline measurement, 300 s of association, 300 s of dissociation. All measurements of Env-Ab binding were corrected by subtracting the background signal obtained from Env traces generated with an irrelevant negative control IgG.

Kinetic analyses were performed by BLI using recombinant Fabs loaded onto FAB2G biosensors (ForteBio, Cat#: 18-5126) (@ 40 ug/ in 1XPBS) and 2-fold dilutions of Env monomers. The assay parameters are the same as for measuring the binding of IgG, but with an extended dissociation phase of 600 s. Curve fitting was used to determine relative apparent antibody affinities for envelope was performed using a 1:1 binding model and the data analysis software (ForteBio). Mean k_{on}, k_{off}, and K_D values were determined by averaging all binding curves within a dilution series having R^2 values of greater than 95% confidence level.

Plasma and antibody ELISA

Plasma samples were heated inactivated at 56°C for 1 h, centrifuged at 13,000 RPM for 10 min at stored at 4°C or −20°C. ELISAs were done in a 384 well plate format. 30 ul of protein at 0.1 uM in coating buffer (0.1M sodium bicarbonate, pH: 9.4-9.6) was added to each well and incubated a room temperature overnight. Plates were washed 4x with ELISA wash buffer (1XPBS + 0.2% Tween-20). 80 ul of blocking buffer (1X PBS + 10% non-fat milk + 0.03% Tween20) was added to the plates and they were incubated at 37°C for 1-2 h. Plates were then washed 4x with ELISA wash buffer. Plasma was diluted 1:10 in blocking buffer and diluted 1:3 across or down the plate. His tag control started at 1 mg/mL. The plates were incubated for 1 h at 37°C. The plates were washed 4x with ELISA was buffer. 30 ul of secondary antibody was added to each well. The plates were incubated for an h at 37°C. Plates were washed 4x with ELISA wash buffer. Following washing 30 ul of SureBlue Reserve TMB Microwell Peroxidase Substrate: KPL (Cat #: 53-00-02) was added to each well. The plates were incubated for 5 min at room temperature. 30 ul of 1N H_2SO_4 was added to each well. Plates were read immediately on the SpectraMax M2 microplate reader (Molecular Devices) at 450 nm. Blank wells were used to subtract the background signal in the analysis.

Single cell sorting

Spleen samples from −80°C were thawed in 37°C water bath until a small ice pellet remained in the sample tube. Then warm (37°C) RPMI was added dropwise to the samples. Cells were then spun down at 300xg for 5 min and washed with 20ml FACs buffer (1x PBS containing 2% FBS and 1mM EDTA) once and then re-suspended in the remaining drop of FACs buffer after decantation.

Cells were then incubated with 1 pmol PE-DL650 and 3 pmols APC-DL755(decoys) for 5 min at room temperature and then 1 pmol PE-antigen tetramer and 1 pmol APC-antigen_knock out (KO) tetramer for 25 min on ice in dark. Tetramers were made by combining biotinylated Env with Streptavidin conjugated to either a PE or APC fluorophore (Prozyme, PJFS25 and PJ27S). Cells were then washed with FACs buffer once and then re-suspended in remaining drop of FACs buffer after decantation. 50 ul anti-PE MicroBeads

and 50 ul anti-APC MicroBeads (Miltenyi Biotec) were then added to the cells and they were incubated for 15-30 min on ice. Cells bound with PE and/or APC were then enriched based on MACS cell separation manual.

Antigen-enriched samples were then stained with the following list of antibody-fluorophore conjugates: IgG1 FITC (BD Biosciences Cat#: 553443, 1:100 dilution), IgG2b FITC (BD Biosciences Cat#: 553395, 1:50 dilution), IgG2c FITC (Bio-Rad Cat#: STAR135F, 1:100 dilution), IgG3 FITC (BD Biosciences Cat#: 553403, 1:400 dilution), IgD PerCP-Cy5.5 (Biolegend Cat#: 405710, 1:180 dilution), Fixable viability stain BV510 (Affymetrix Cat#: 65-0866-14, 1:200 dilution), CD3 BV510 (BD Biosceinces Ct#: 564024, 1:50 dilution), CD4 BV510 (BD Biosciences Cat#: 563106, 1:100 dilution), Gr-1 BV510 (BD Biosciences Cat#: 563040, 1:200 dilution), F4/80 BV510 (BD Biosciences Cat#: 123135, 1:50 dilution), IgM BV605 (Biolegend Cat#: 406523, 1:50 dilution), CD19 BV650 (BD Bioscience Cat#: 563235, 1:100 dilution), and B220 BV786 (BD Bioscience Cat#: 563894, 1:100 dilution). Cells were stained for 30 min on ice in the dark. Cells were then washed 3 times with 2 mL of FACs buffer wash. Samples were then re-suspended in 1-2 mL of FACs buffer.

Naive, antigen-specific B cells were sorted as CD3-, CD4-, Gr-1-, F4/80-, B220+, CD19+, antigen+/antigen KO-. Class-switched IgG B cells from immunized animals were sorted based on the following markers: CD3-, CD4-, Gr-1-, F4/80-, B220+, CD19+, IgM-, IgD-, IgG1+, IgG2b+, IgG2c+, IgG3+, antigen+/antigen KO- (Figure S4). Individual B cells were sorted using the FACS ARIA II into a 96 well plate containing lysis buffer, as previously reported (Parks et al., 2019). The number of cells sorted from each immunization group is now indicated in Table S6.

VH and VL amplification and sequencing

The amplification and sequencing of VH and VL genes were performed as previously described (Parks et al., 2019). For light chain PCR reactions, 15 ul of cDNA and 15 ul of first round PCR product were used. 7 ul of cDNA or PCR product was used for the heavy chain PCR reactions. Samples were sequenced using Sanger sequencing (Genewiz, Seattle, WA) and sequence analysis was performed as previously described (Parks et al., 2019). Amino acid and nucleotide mutations were identified by aligning the VH and VL gene sequences to the corresponding germline genes (IMGT Repertoire) using the Geneious Software (Version 8.1.9). For VL, mutations were counted beginning at the CDR1 of the V-gene to the 3¢ end of FW3. For VH, mutations were counted beginning at the CDR1 of the V-gene to the end of the CDR3. The number of sequences obtained from each immunization group is summarized in Table S6.

Monoclonal antibody production

Gene-specific PCR was used to amplify the DNA product from the first round PCR using primers designed to anneal to the gene of interest as well as add ligation sites to facilitate insertion of the DNA fragment into the human IgG1 vector [ptt3 k for kappa (Snijder et al., 2018), and PMN 4-341 for gamma (Mouquet et al., 2010)]. Each gene specific PCR reaction contained 0.5 ul each of 10 uM 5¢ and 3¢ primer, 22.5 ul Accuprime Pfx Supermix (Cat#: 12344040), and 1.5 ul of 1st or 2nd round PCR product. The gene-specific PCR product was infused into the cut IgG1 vector in a reaction containing 12.5 ng of cut vector, 50 ng of insert, 0.5 ul of 5X Infusion enzyme (InFusion HD Cloning Kit, Cat#: 639649), and nuclease-free water to bring volume to 2.5 ul. The entire reaction was used to transform competent *E. coli* cells and plated on agar plates containing ampicillin. DNA was prepared using QIAprep Spin Miniprep Kit (QIAGEN, Cat#: 27106). Equal amounts of heavy and light chain DNA and 293F transfection reagent (Millipore Sigma, Cat#: 72181) were used to transfect 293E cells. 5-7 days post transfection cell supernatants were collected, and the antibodies were purified using Pierce Protein A agarose beads (ThermoFisher, Cat#: 20334). The antibodies were eluted using 0.1 M Citric Acid into a tube containing 1 M Tris. The antibodies were buffer exchanged into 1XPBS using an amicon centrifugal filter.

To make Fabs, the IgG was cleaved overnight at 37þC to generate antigen binding fragment (Fab) with Endoproteinase Lys-C (NEB). To remove undigested IgG and IgG Fc fragments, the mixture was incubated with Protein A Agarose Resin for 1 h at room temperature. Beads were washed with 1X PBS to remove excess Fab. Fab was further purified on SEC using a HiLoad 16/600 Superdex 200 pg (GE) column.

QUANTIFICATION AND STATISTICAL ANALYSIS

Mean and standard deviations were calculated using R (Version 3.4.1). Statistical analyses were calculated using R (Version 3.4.1) (R Core Team, 2018) and GraphPad Prism. Descriptions of the statistical methods used for each dataset are described in the figure legends. The tidyverse packages (Wickham, 2017) were used in R to manipulate data and create graphs in addition to GraphPad Prism. WebLogo was used to generate the logo plots (Crooks et al., 2004).